Project Number: MQP-ECE-AEE-PSS6

Non-Invasive Transmission Line Fault Identification and Location Detection

A Major Qualifying Project Proposal
Submitted to the Faculty of
WORCESTER POLYTECHNIC INSTITUTE
In Partial Fulfillment of the Requirements for the
Degree of Bachelor of Science
By

Caitlin Slezycki

Approved By:

Professor Alexander Emanuel, Advisor

11 January 2008

Abstract

This project explores the theoretical application of a method of identifying and locating transmission line faults through the use of magnetic fields. Using Faraday's law and Ampère's law, this project demonstrates that transmission line faults can be detected and identified by category of disturbance. The voltage-current relationship established in electromagnetic field theory enables to monitor the line currents and detect a fault. This method can also be used to determine the location of the fault over the transmission line length.

Acknowledgements

I, the author of this report, would like to thank my advisor Professor Alexander Emanuel for his support in this project. Additionally, I would like to thank the Electrical and Computer Engineering Department of Worcester Polytechnic Institute. Finally, I would like to thank my family, especially my father, for their continuing love and support.

Caitlin Slezycki
January 2008

Table of Contents

ABSTRACT ..... **ii**

ACKNOWLEDGEMENTS ..... **iii**

TABLE OF CONTENTS ..... **iv**

TABLE OF FIGURES ..... **v**

LIST OF TABLES ..... **vi**

1 INTRODUCTION **1**

2 BACKGROUND **2**

2.1 INTRODUCTION 2
2.2 TRANSMISSION SYSTEM 2
2.3 POWER SYSTEM FAULT 4
2.4 FAULT LOCATION ACCURACY 6
2.5 FAULT LOCATION TECHNIQUES 7
2.5.1 Phasor Based Algorithms Method *7*
2.5.2 Traveling Wave Method *9*

3 SYSTEM DEVELOPMENT **10**

3.1 PROPOSED SYSTEM 10
3.2 PROOF OF CONCEPT 10
3.2.1 Magnetic Field Application in Fault Detection and Location *10*

4 SYSTEM DESIGN **14**

4.1 FAULT DETECTOR 14
4.1.1 Single Phase System *14*
4.1.2 Three Phase System *22*
4.2 FAULT LOCATOR 29

5 SYSTEM SIMULATION AND ANALYSIS **32**

5.1 FAULT DETECTOR 32
5.1.1 Single Phase System *32*
5.1.2 Three Phase System *41*
5.2 FAULT LOCATOR 52

6 CONCLUSIONS AND FUTURE RECOMMENDATIONS **55**

REFERENCES **56**

APPENDICES **58**

APPENDIX A – LIST OF SYMBOLS 58
APPENDIX B – LIST OF CONSTANTS 59
APPENDIX C – SINGLE PHASE RMS VOLTAGES GRAPH DATA 60
APPENDIX D – PSPICE PHASE TO GROUND SCHEMATICS 61
APPENDIX E – PSPICE TWO PHASE TO GROUND SCHEMATICS 62
APPENDIX F – PSPICE THREE PHASE TO GROUND SCHEMATIC 63
APPENDIX G – PSPICE PHASE TO PHASE SCHEMATICS 64

Table of Figures

FIGURE 2.1: BASIC STRUCTURE OF THE BULK POWER SYSTEM 2
FIGURE 2.2: SYSTEM PROTECTION IN NORMAL OPERATION 5
FIGURE 2.3: SYSTEM PROTECTION DURING FAULT CLEARING 5
FIGURE 3.1: MAGNETIC FIELD AROUND A WIRE 11
FIGURE 3.2: MAGNETIC FIELD AROUND A TRANSMISSION WIRE 12
FIGURE 4.1: SINGLE PHASE TRANSMISSION DESIGN 14
FIGURE 4.2: DIMENSIONS OF SINGLE PHASE TRANSMISSION DESIGN 15
FIGURE 4.3: WAVEFORM OF SINGLE PHASE SYSTEM 16
FIGURE 4.4: FAULT DETECTOR ORIENTATION ON TRANSMISSION TOWER 18
FIGURE 4.5: INDUCED VOLTAGE OF FAULT DETECTOR 18
FIGURE 4.6: MAGNETIC FIELD INTENSITY OF FAULT DETECTOR 19
FIGURE 4.7: MAGNETIC FIELD INTENSITY VECTOR COMPONENTS 19
FIGURE 4.8: THREE PHASE TRANSMISSION DESIGN 22
FIGURE 4.9: DIMENSIONS OF THREE PHASE TRANSMISSION DESIGN 23
FIGURE 4.10: PHASE ANGLES OF THREE PHASE SYSTEM 25
FIGURE 4.11: WAVEFORM OF THREE PHASE SYSTEM 25
FIGURE 4.12: PHASE A MAGNETIC FIELD INTENSITY 26
FIGURE 4.13: PHASE B MAGNETIC FIELD INTENSITY 26
FIGURE 4.14: PHASE C MAGNETIC FIELD INTENSITY 26
FIGURE 4.15: THREE PHASE TOTAL MAGNETIC FIELD INTENSITY 28
FIGURE 4.16: FAULT LOCATION SCHEME IN A TRANSMISSION SYSTEM 29
FIGURE 5.1: SINGLE PHASE TRANSMISSION DESIGN WITH PARAMETERS 33
FIGURE 5.2: GRAPH OF SINGLE PHASE VERTICAL AND HORIZONTAL RMS VOLTAGES 36
FIGURE 5.3: PSPICE SINGLE PHASE TRANSMISSION SCHEMATIC 38
FIGURE 5.4: PSPICE SINGE PHASE TRANSMISSION MAGNETIC FIELD INTENSITY 38
FIGURE 5.5: PSPICE SINGLE PHASE TRANSMISSION FAULT SCHEMATIC 39
FIGURE 5.6: PSPICE SINGE PHASE TRANSMISSION FAULT MAGNETIC FIELD INTENSITY 39
FIGURE 5.7: THREE PHASE TRANSMISSION DESIGN WITH PARAMETERS 41
FIGURE 5.8: PSPICE THREE PHASE TRANSMISSION SCHEMATIC 44
FIGURE 5.9: PSPICE THREE PHASE TRANSMISSION H_A MAGNETIC FIELD INTENSITY 44
FIGURE 5.10: PSPICE THREE PHASE TRANSMISSION H_B MAGNETIC FIELD INTENSITY 45
FIGURE 5.11: PSPICE THREE PHASE TRANSMISSION H_C MAGNETIC FIELD INTENSITY 45
FIGURE 5.12: PSPICE THREE PHASE TRANSMISSION $H_{X,TOTAL}$ AND $H_{Y,TOTAL}$ MAGNETIC FIELD INTENSITY 46
FIGURE 5.13: PSPICE PHASE A TO GROUND $H_{X,TOTAL}$ AND $H_{Y,TOTAL}$ MAGNETIC FIELD INTENSITY 47
FIGURE 5.14: PSPICE PHASE B TO GROUND $H_{X,TOTAL}$ AND $H_{Y,TOTAL}$ MAGNETIC FIELD INTENSITY 47
FIGURE 5.15: PSPICE PHASE C TO GROUND $H_{X,TOTAL}$ AND $H_{Y,TOTAL}$ MAGNETIC FIELD INTENSITY 48
FIGURE 5.16: PSPICE PHASE A TO PHASE B TO GROUND $H_{X,TOTAL}$ AND $H_{Y,TOTAL}$ MAGNETIC FIELD INTENSITY 48
FIGURE 5.17: PSPICE PHASE B TO PHASE C TO GROUND $H_{X,TOTAL}$ AND $H_{Y,TOTAL}$ MAGNETIC FIELD INTENSITY 49
FIGURE 5.18: PSPICE PHASE A TO PHASE C TO GROUND $H_{X,TOTAL}$ AND $H_{Y,TOTAL}$ MAGNETIC FIELD INTENSITY 49
FIGURE 5.19: PSPICE THREE PHASE TO GROUND $H_{X,TOTAL}$ AND $H_{Y,TOTAL}$ MAGNETIC FIELD INTENSITY 50
FIGURE 5.20: PSPICE PHASE A TO PHASE B $H_{X,TOTAL}$ AND $H_{Y,TOTAL}$ MAGNETIC FIELD INTENSITY 50
FIGURE 5.21: PSPICE PHASE B TO PHASE C $H_{X,TOTAL}$ AND $H_{Y,TOTAL}$ MAGNETIC FIELD INTENSITY 51
FIGURE 5.22: PSPICE PHASE A TO PHASE C $H_{X,TOTAL}$ AND $H_{Y,TOTAL}$ MAGNETIC FIELD INTENSITY 51
FIGURE 5.23: FAULT LOCATION SCHEME IN A TRANSMISSION SYSTEM 52

List of Tables

TABLE 4.1: SINGLE PHASE TRANSMISSION DESIGN DIMENSIONS DESCRIPTIONS 16
TABLE 4.2: FAULT DETECTOR COMPONENTS 19
TABLE 4.3: THREE PHASE TRANSMISSION DESIGN DIMENSIONS DESCRIPTIONS 24
TABLE 4.4: COMPONENTS IN FAULT LOCATION SCHEME 29
TABLE 5.1: SINGLE PHASE TRANSMISSION DESIGN PARAMETER DESCRIPTIONS 33
TABLE 5.2: VARIABLE ASSIGNMENT FOR SINGLE PHASE INDUCED VOLTAGE EQUATION 35
TABLE 5.3: THREE PHASE TRANSMISSION DESIGN PARAMETER DESCRIPTIONS 42
TABLE 5.4: COMPONENTS IN FAULT LOCATION SCHEME 52

1 Introduction

Electricity is a vital commodity that economies and citizens rely on. It is necessary to have a dependable electric delivery system capable of accommodating the increasing demand for electricity.

A short circuit fault is one of the most extreme conditions of the delivery system. If not cleared promptly, short circuit faults may damage the equipment, endanger the personnel, and jeopardize the system stability [3]. However, the extent of the fault's damage on the transmission system depends on the ability to promptly identify and accurately locate a fault. The need for a method that quickly and reliably locates a fault has not been unnoticed. Many authors have researched this topic and have proposed valuable methods [3]. These methods can be categorized as either a phasor based algorithm scheme or traveling wave scheme. Although these techniques have proven to successfully locate a fault, the accuracy of the location is often inadequate due to the collection of faulty data directly from the transmission line or assumptions made in calculations.

This project explores the theoretical application of a proposed fault identification and location method by analyzing magnetic fields. The voltage-current relationship established in magnetic field theory enables the ability to monitor the transmission line currents to detect and identify a fault. The time when a fault is detected is then used for calculating the location of the fault. This method proves to be a more accurate approach to fault location due to its non-invasive technique.

This method is evaluated by simulations of single phase and three phase circuits. By simulating these models, the capability of using magnetic field theory to identify and locate faults is verified.

2 Background

2.1 Introduction

This section describes transmission systems, faults, and current fault identification and location techniques. Familiarity with these topics aids in the understanding of later sections.

2.2 Transmission System

The electric delivery system (transmission system) is one of the greatest engineering achievements of the 20th century [1, 13]. It is an extensive system of interconnected networks in which electric power is delivered reliably and economically from generators to loads. More specifically, electricity is produced at generators and is then stepped up by transformers for transportation across high voltage transmission lines. These lines are interconnected at switching stations and substations to form a network of lines and stations called a power "grid". At substations, transformers step the electric voltage down for distribution to customers through lower voltage distribution lines. As shown in Figure 2.1, these generation and transmission components make up the "bulk power system".

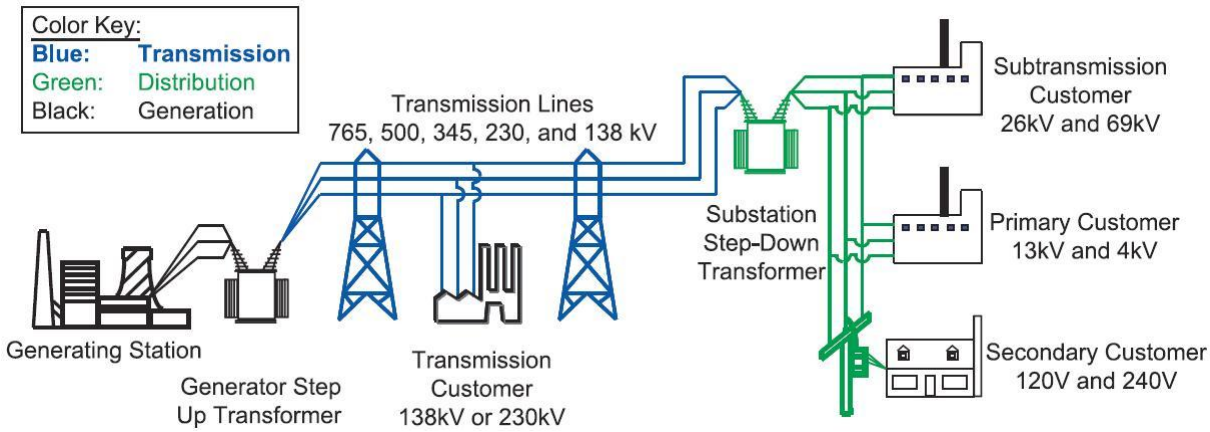

Figure 2.1: Basic Structure of the Bulk Power System [2]

Due to the great dependence on power delivery, the transmission system is expected to maintain its integrity and continue to operate properly without a major disruption even when a component fails [2]. To assure transmission system reliability and security, councils such as the North America Electric Reliability Council (NERC[1]), the Western Systems Coordinating Council (WSCC[2]), and the Electric Reliability Council of Texas (ERCOT[3]) have developed criteria for the system's operation. Transmission systems operate in one of three states: normal, emergency, or restorative. The ideal operation is in a normal state where the frequency of the system stays within acceptable bounds, all voltages at all locations are within required ranges, no component is overloaded beyond its appropriate rating, and no load is involuntarily disconnected [2]. However, there are circumstances when failures in the system occur, resulting in non-ideal state operation. One circumstance is when a conducting path (short circuit) is created. This undesirable occurrence is known as a fault and results in emergency state system operation. Once the emergency state is detected the system can be realigned to isolate the affected line and reroute current to the loads. This is the restorative state.

[1] NERC's mission is to improve the reliability and security of the bulk power system in North America. To achieve that, NERC develops and enforces reliability standards; monitors the bulk power system; assesses future adequacy; audits owners, operators, and users for preparedness; and educates and trains industry personnel. NERC is a self-regulatory organization that relies on the diverse and collective expertise of industry participants. As the Electric Reliability Organization, NERC is subject to audit by the U.S. Federal Energy Regulatory Commission and governmental authorities in Canada.

[2] The Western Electricity Coordinating Council ("WECC") is a Utah nonprofit corporation with the mission to do the following consistent with these Bylaws:

1. Maintain a reliable electric power system in the Western Interconnection that supports efficient competitive power markets ("Reliability Mission"); and
2. Assure open and non-discriminatory transmission access among Members and provide a forum for resolving transmission access disputes between Members ("Transmission Access Mission").

[3] The mission of the Electric Reliability Council of Texas (ERCOT) is to direct and ensure reliable and cost-effective operation of the electric grid and to enable fair and efficient market-driven solutions to meet customers' electric service needs.

2.3 Power System Fault

A short circuit fault represents one of the most extreme conditions of the power system [3]. Faults most often occur during severe weather conditions when lightning strikes towers or conductors. This causes stress on the insulation between the transmission conductors and supporting structures. Faults are additionally caused by some natural events such as birds colliding with transmission lines, wind damage, trees falling across lines, vehicles colliding with towers or poles, aircrafts colliding with lines, and excessive ice loading. A fault can be categorized as one of four types: phase to ground, two phases to ground, three phase to ground, and phase to phase. The most common fault is a phase to ground fault occurring when an electric path between the ground and any of the line conductors is formed (phase to ground) or a path between any two conductors jointly connected to the ground is formed (two phase to ground). Additionally, all three conductors can be involved in a three phase ground fault (three phase to ground). When a fault between the conductors without involving a ground connection occurs, it is called a phase to phase fault [14].

When a fault occurs, it requires that the line be taken out of service immediately to prevent further expansion of the problem or damage to system components. This operation is provided by protective equipment that detects and clears faults, restoring reliable function quickly. The primary system protection components include measuring devices, protective relays, control equipment, and circuit breakers. This protection scheme in normal operation is shown in Figure 2.2. A fault in a line is detected by equipment called protective relays that issue a trip command to the switching equipment (circuit breakers) to open both ends of a transmission line if a fault is detected and confirmed by the relays [14]. An illustrative

example of fault clearing is shown in Figure 2.3. Relay systems are designed to operate automatically and more or less instantaneously [2]. This process of rapid and efficient power restoration depends on quick and accurate fault location.

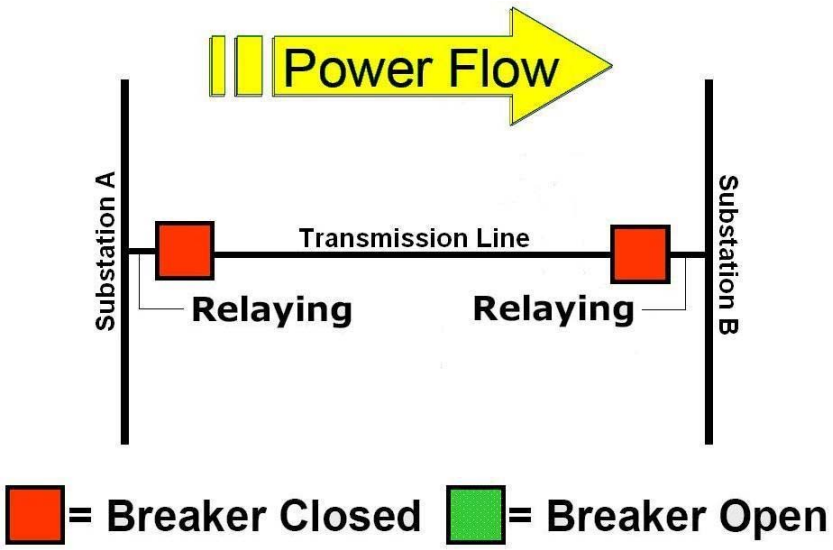

Figure 2.2: System Protection in Normal Operation

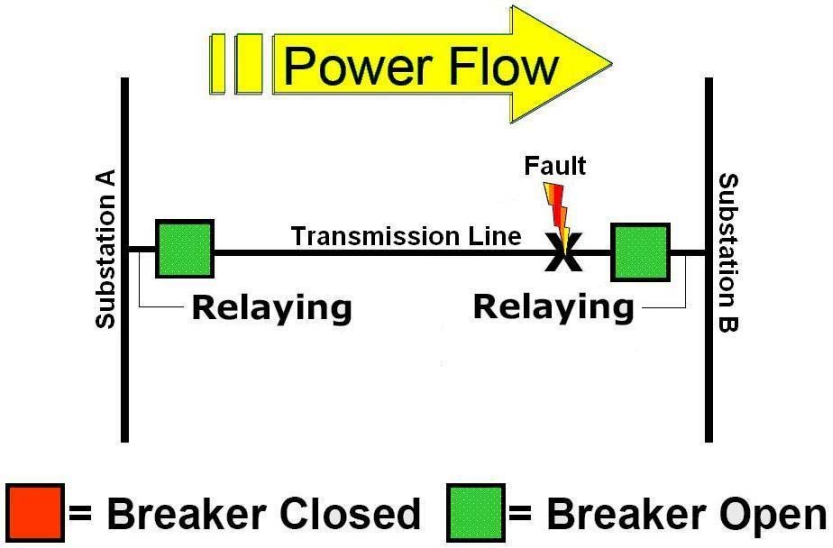

Figure 2.3: System Protection during Fault Clearing

2.4 Fault Location Accuracy

In determining the most appropriate fault location method, it is vital to consider the performance of a system in the application which it is being utilized. Even though fault location implementation can be diverse, it should be noted that accuracy is one of the key elements to consider. It is essential to understand the possible benefits and shortcomings of using different types of data and system implementation approaches when designing or selecting a fault locator [14].

Accurate location of faults on power transmission systems can save time and resources for the electric utility industry. Line searches for faults can be inconclusive. Accurate information needs to be acquired quickly in a form most useful to the power system operator communicating to field personnel [1]. There are certain requirements that fault location schemes attempt to satisfy. These requirements, according to Webster[4], are as follows:

- The accuracy must be sufficient to locate the fault within a span of two towers. Typically 0.1% error is acceptable, but an accuracy of 0.01% is desirable.
- The accuracy should be maintained even if only a short segment of the fault data from a distorted waveform is measured. Typically, it is required that no more than a few cycles of data are sufficient for the calculation.
- The accuracy should not deteriorate if various types of faults and numerous auto-reclosing requirements are considered. Typically, it is acceptable if the accuracy deteriorates under some difficult fault causes in which the fault

[4] Webster, John G. "Fault Location." Wiley Encyclopedia of Electrical and Electronics Engineering. New York: John Wiley & Sons, Inc., 1999.

resistance changes during the fault, but it is desirable that the accuracy be stable even under these conditions.

An ideal fault location scheme would have an accuracy that is able to fulfill these requirements. The increased accuracy provides for more reliable and efficient restoration of power to customers.

2.5 Fault Location Techniques

Fault location techniques are used in determining the location of a fault on a transmission line. Once a fault is located, the damage caused by the fault can be repaired and power can be restored. The efficiency by which this is executed heavily relies on the ability to accurately locate a fault. The technique used for fault location has been a subject of interest over the years resulting in the development of several fault location schemes. Current common methods include the phasor based algorithm approach and the traveling wave approach.

2.5.1 Phasor Based Algorithms Method

This approach to fault location utilizes phasor based algorithms in which only the fundamental components of signals are used. The algorithms use a Fourier transform to model the line, where the line is represented by its length and its impedance per unit length. The approach used in phasor based algorithms involves measuring the voltage and current phasors, extracting the fundamental components, determining the phasors and fault type, and applying impedance algorithms. In phasor based algorithms, the location where measurements are taken must be taken into consideration. The more common one terminal algorithms use measured data from one side (sending end) of the line while two terminal algorithms use data from both the sending and receiving end. However, the need for

communication between the sending and receiving end of two-terminal algorithms makes it a less desirable choice.

The single terminal method is a standard feature in most numerical relays. This approach uses a simple algorithm in which no communication channels or remote data are required. Although this approach provides reasonable results, certain errors occur in fault location calculation due to inherent assumptions. This is evidenced in the proposed approaches to the method. Westlin first introduced a scheme for single terminal lines using the Newton-Raphson method to solve the related nonlinear equations. However, due to the large number of necessary computations, equations in this method use scaled down components for simplification. In attempt to create a more reliable result, Takagi created a method that uses superimposed components for long line modeling. This method also uses the fault current distribution factor, which is assumed to be real. The assumptions used in single terminal algorithms create results that may cause errors in fault location.

The more reliable phasor based algorithm is that of two terminals. Two terminal algorithms use fewer assumptions resulting in more reliable calculations. One method of a two terminal algorithm application is a method that was introduced in 1999 that uses negative sequence quantities from all line terminals for the location of unbalanced faults [15]. This use of negative sequence quantities makes it possible to negate the effect of prefault load and fault resistance, zero sequence, mutual impedance, and zero sequence infeed from transmission taps. Additionally, this approach additionally does not require data alignment because the algorithm at each of the two terminals uses values from the remote terminal.

2.5.2 Traveling Wave Method

Another common fault location technique that has been developed is the traveling wave method. This method attempts to improve the accuracy of fault location using a limited amount of available data. When a fault occurs, transient signals are generated that travel through the transmission line as waves. These waves are high frequency electromagnetic impulses that are a result of abrupt changes in the voltage at the fault. The waves travel away from the fault in both directions towards the line's end terminals. The fault is located by time-tagging the arrival of the wave at each end of the line and then multiplying the wave velocity by the time difference in line ends [9, 12].

There are many benefits to the use of the traveling wave method in comparison to the phasor based algorithm approach. Unlike phasor based algorithms, the traveling wave method is unaffected by load conditions, high ground resistance, and series capacitor banks. It provides more accurate fault location through the accurate time-tagging of wave arrival at line end terminals. This technique is becoming more widely used since the introduction and availability of affordable global positioning systems (GPS). The necessity of fast, reliable, and accurate data acquisition in this method is, however, crucial to its effectiveness. The implementation of this method would require a potentially complex upgrade to the system.

3 System Development

3.1 Proposed System

The dependence on reliable fault detection and location warrants the investigation and development of increasingly accurate and time efficient methods of fault detection. The proposed method explores the application of magnetic fields in fault detection. The voltage-current relationship in magnetic fields can be used for the monitoring of current in transmission lines. This method has the ability to differentiate between the desired current flow and when the current equals zero, otherwise known as a fault. As stated above, if a fault is observed (detected), it is vital to determine the exact location and type of the fault. The proposed method for fault location is based on calculations of the fault detection time and line length.

The proposed fault detector and fault locator methods are described in further detail in the remaining sections of this paper.

3.2 Proof of Concept

Magnetic fields exist in the space around wires that carry current in which the basic source of the magnetic field is the electrical charge in motion [7]. This relationship between a magnetic field and current validates the need for research of the application of magnetic fields in fault detection and identification and fault location schemes.

3.2.1 Magnetic Field Application in Fault Detection and Location

A magnetic field is composed of lines of magnetic flux that form closed paths as illustrated in Figure 3.1. Flux lines are close together where the field is strong and farther apart where the field is weak. The magnetic flux (ϕ) passing through a surface area (A) can

be determined using the magnetic flux density vector (**B**). The flux density vector **B** has a direction perpendicular to the flux lines as shown in Figure 3.1. The resulting equation for magnetic flux is noted in Equation 3.1.

$$\phi = \mathbf{B}A \quad \text{(Wb)} \tag{3.1}$$

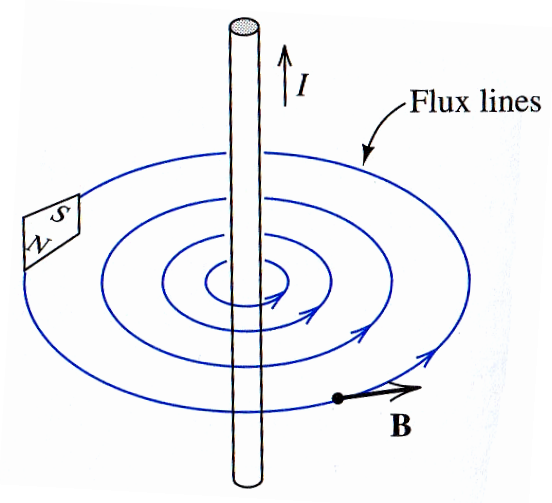

Key:
I = Current
B = Magnetic Flux Density
S = South-Seeking End of Magnet
N = North-Seeking End of Magnet

Figure 3.1: Magnetic Field Around a Wire [7]

In a coil that has N turns, the total flux linkages (λ) are given by Equation 3.2 where N is the number of turns, ϕ is the instantaneous value of a time-varying flux, and A is area.

$$\lambda = N\phi = N(\mathbf{B}A) \quad \text{(Wb} \cdot \text{turns)} \tag{3.2}$$

According to Faraday's law of magnetic induction, the magnetic flux density induces a voltage in a coil if the flux linkages are changing with time [7]. Hence, the voltage induced in the coil in Faraday's law, is given by Equation 3.3.

$$e = \frac{d\lambda}{dt} = NA\frac{d\mathbf{B}}{dt} \quad \text{(V)} \tag{3.3}$$

The relationship between a magnetic field and current is formulated by Ampère's law which states that the line integral of the magnetic field intensity around a closed path is equal to the algebraic sum of the currents (i) flowing through the area enclosed by the path [7]. Ampère's law is given in Equation 3.4 in which $\mathbf{dl}$ is a vector element of length that is perpendicular to the path of integration and $\mathbf{H}$ is a vector element of magnetic field intensity that is determined by currents flowing in coils and the configuration of those coils.

$$\oint \mathbf{H} \cdot d\mathbf{l} = \sum i \tag{3.4}$$

However, if the magnetic field intensity has constant magnitude and points in the same direction as the incremental length $d\mathbf{l}$ everywhere along the path, Ampère's law reduces to that given in Equation 3.5 [7].

$$Hl = \sum i \tag{3.5}$$

In long straight lines of wire such as transmission lines that carry current, the magnetic field can be determined with Ampere's law and symmetry as illustrated in Figure 3.2.

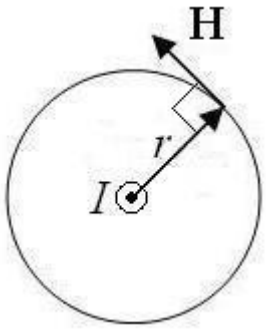

Figure 3.2: Magnetic Field around a Transmission Wire

In this application, the magnetic field intensity (**H**) and magnetic flux density (**B**) are in a plane perpendicular to the wire and the magnitude of H is constant for a given radius r.

Ampère's law (Equation 3.5) can be applied to the system as shown in Equation 3.6 from which the system's magnetic intensity can be solved as shown in Equation 3.7.

$$Hl = H2\pi r = I \quad \text{(A)} \tag{3.6}$$

$$H = \frac{I}{2\pi r} \quad \text{(A/m)} \tag{3.7}$$

Furthermore, the magnetic flux density for Figure 3.2 can be solved. The magnetic flux depends on the magnetic field intensity as well as the properties of the material filling the space around the coils of the sensor [7]. The material's magnetic permeability μ will be assumed to be that of free space μ_0, where $\mu_0 = 4\pi \times 10^{-7}$ (Wb/Am). The magnetic field intensity (**H**) and magnetic flux density (**B**) are related as shown by Equation 3.8.

$$\mathbf{B} = \mu \mathbf{H} \quad (\text{Wb/m}^2 = \text{T}) \tag{3.8}$$

Using Equation 3.8, the magnetic flux density of Figure 3.2 can then be calculated as shown in Equation 3.9.

$$B = \mu H = \frac{\mu I}{2\pi r} \quad (\text{Wb/m}^2 = \text{T}) \tag{3.9}$$

Thus, the use of magnetic fields in the application of fault detection and location is a distinct possibility. Utilizing the known relationship between magnetic fields and current, a system that detects faults by monitoring the current in transmission wires with magnetic sensors validates further research.

4 System Design

This section presents the design of the fault detector for single phase and three phase systems and the fault locator.

4.1 Fault Detector

4.1.1 Single Phase System

The proposed fault detector for a single phase design is illustrated in Figure 4.1.

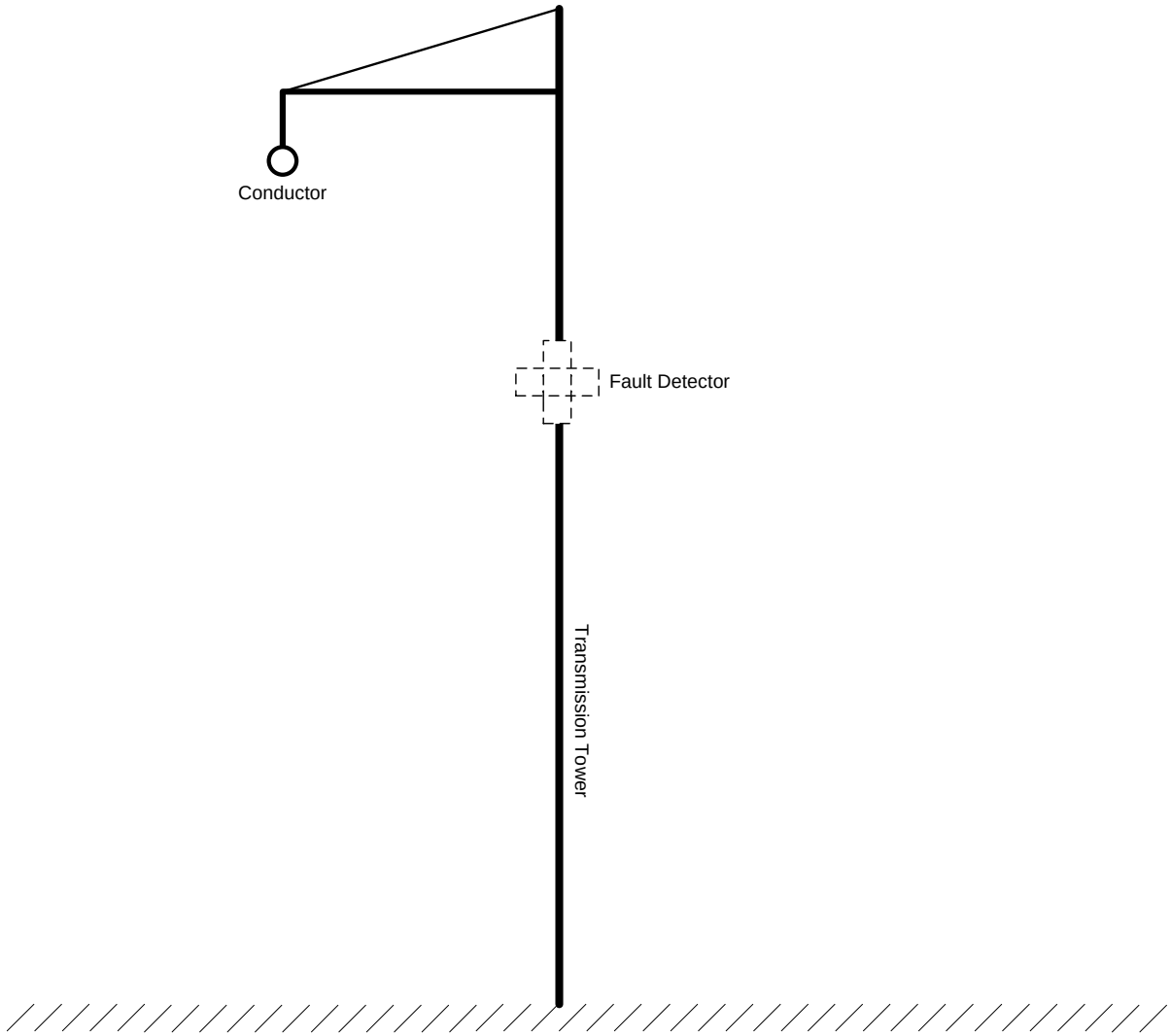

Figure 4.1: Single Phase Transmission Design

The design of Figure 4.1 is defined with additional detail to demonstrate the component measurement using trigonometry as shown in Figure 4.2. The dimensions of Figure 4.2 are defined in Table 4.1.

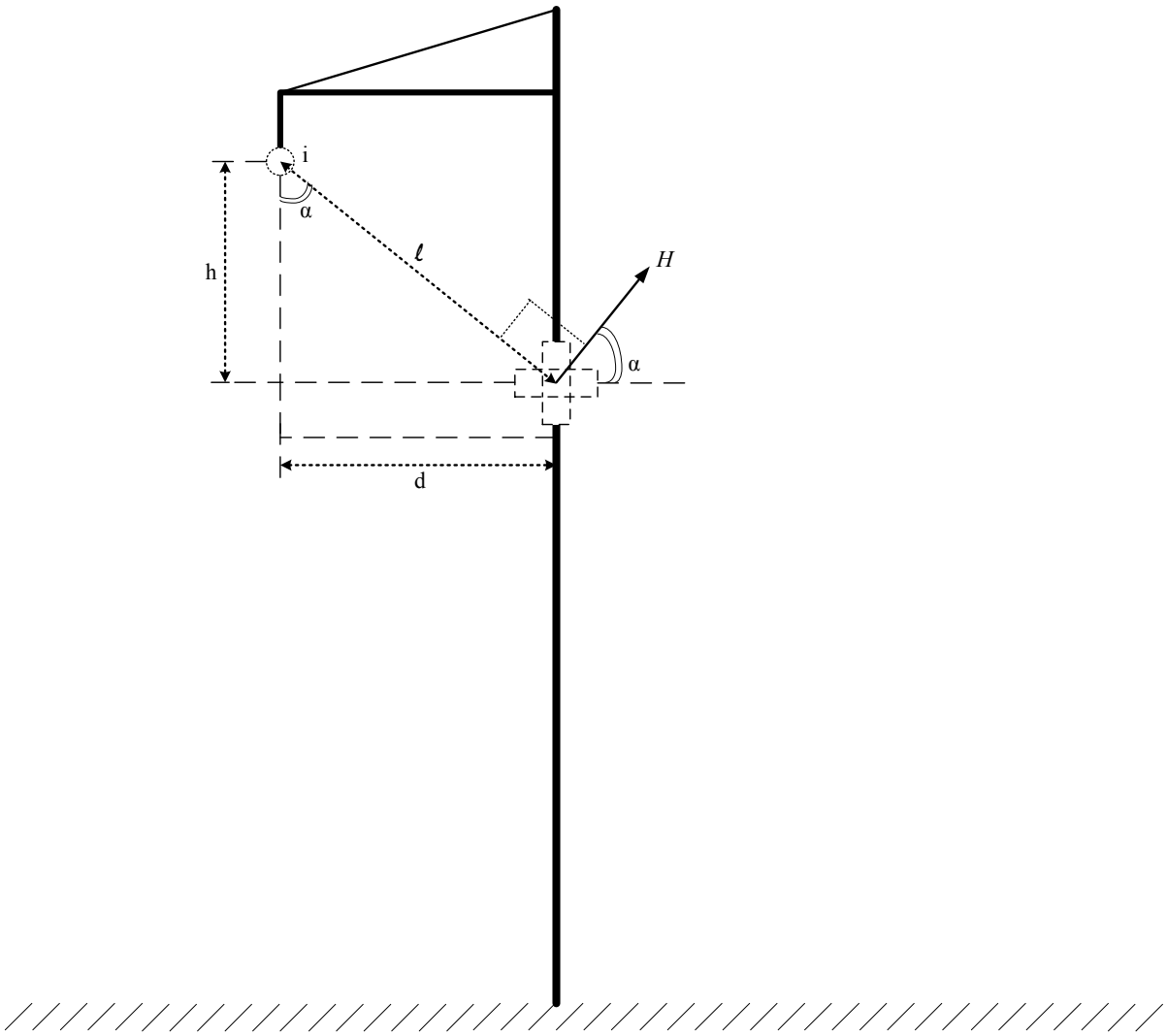

Figure 4.2: Dimensions of Single Phase Transmission Design

Table 4.1: Single Phase Transmission Design Dimensions Descriptions

Dimension Symbol	Dimension Description	Dimension Units
i	Current of Conductor	A
h	Height of Conductor from Fault Detector	m
d	Horizontal Distance of Conductor from Fault Detector	m
ℓ	Length between Conductor and Fault Detector	m
α	Length Measurement ℓ Angle of Approach	Degree (°)
H	Magnetic Field Intensity	A/m

The current of the conductor (*i*) has a sinusoidal value comprised of the maximum current (highest amplitude of the sin wave) I_{MAX} (A) and the frequency of the sin wave ω. This is exemplified in Equation 4.1 and produces a waveform similar to that of Figure 4.3.

$$i = I_{MAX} \sin(\omega t) \quad \text{(A)} \tag{4.1}$$

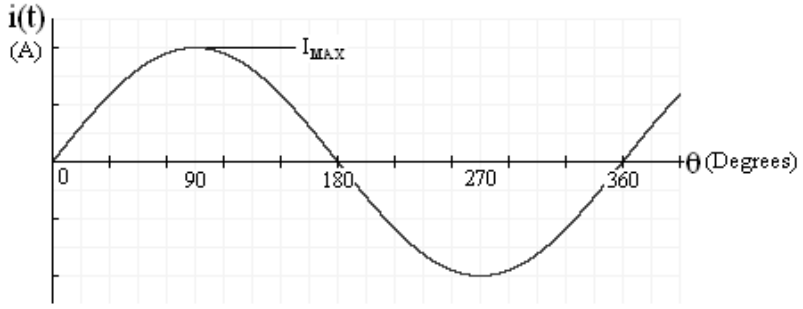

Figure 4.3: Waveform of Single Phase System

From Figure 4.2, the length between the conductor and fault detector ℓ (also referred to as the hypotenuse of the triangle formed between h, d, ℓ) can be found using a variation of the Pythagorean theorem. Since the legs of the triangle (h and d) form a right angle, the equation for the length of the hypotenuse (ℓ) is shown in Equation 4.2.

$$\ell = \sqrt{h^2 + d^2} \quad \text{(m)} \tag{4.2}$$

As shown in Figure 3.2, the angle between the current in a conductor and its magnetic field intensity has a value of 90°, a right angle. Geometry can then be used in analyzing the triangles formed in Figure 4.2. From this analysis, it may be assumed that the triangles are congruent due to the equality of their corresponding sides and angles. This congruency establishes the equality each angle α. Therefore, using trigonometry, it can be noted for future reference that the sine of α is that of Equation 4.3 and the cosine of α is that of Equation 4.4.

$$\sin(\alpha) = \frac{\mathrm{d}}{\ell} \tag{4.3}$$

$$\cos(\alpha) = \frac{\mathrm{h}}{\ell} \tag{4.4}$$

The fault detector of Figure 4.2 is described in more detail in Figure 4.4 – Figure 4.6 with components defined in Table 4.2.

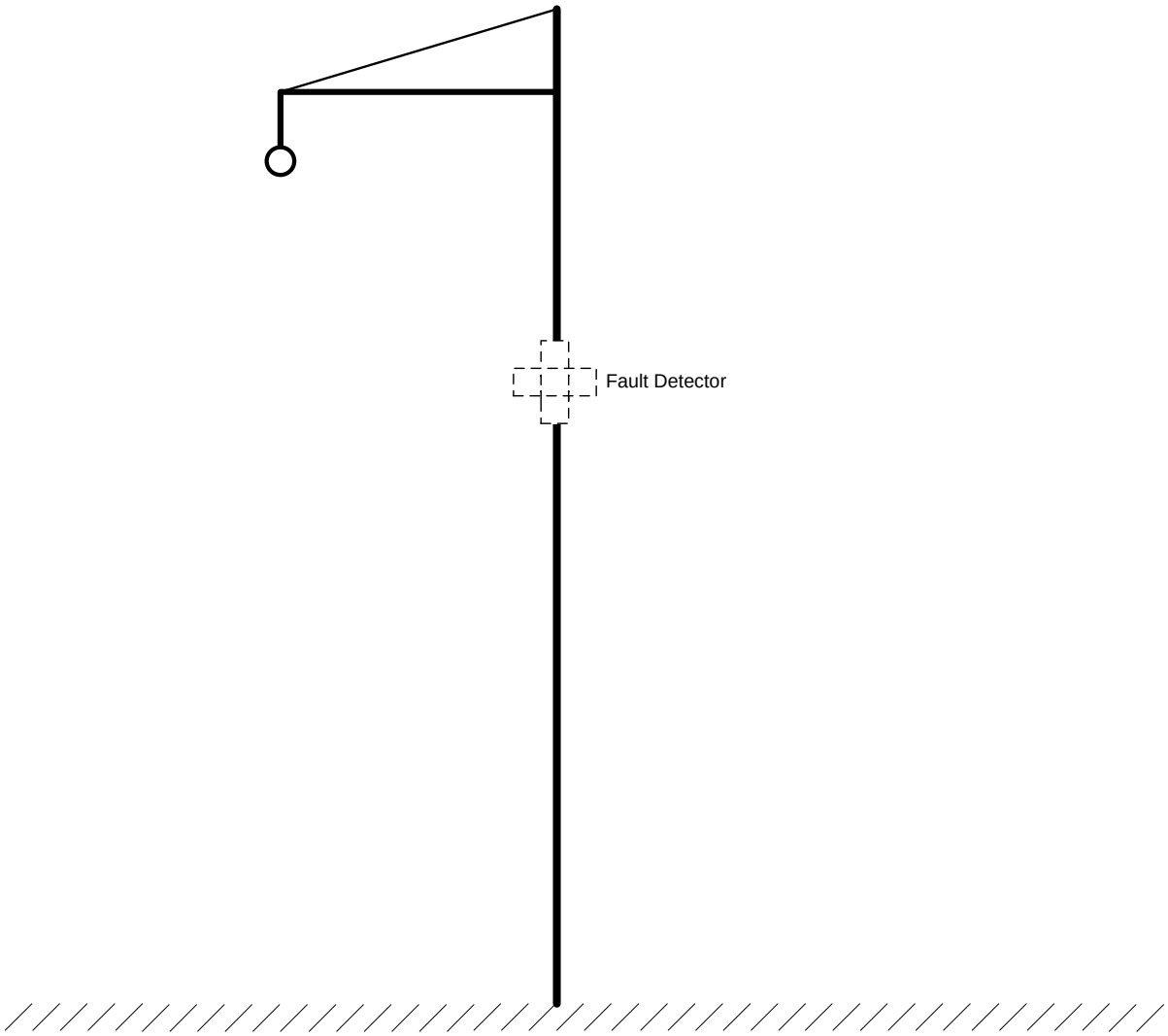

Figure 4.4: Fault Detector Orientation on Transmission Tower

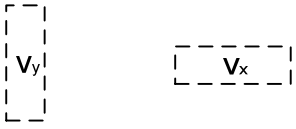

Figure 4.5: Induced Voltage of Fault Detector

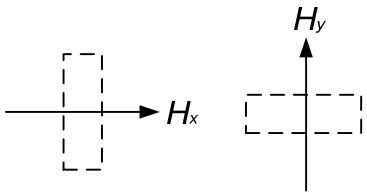

Figure 4.6: Magnetic Field Intensity of Fault Detector

Table 4.2: Fault Detector Components

Dimension Symbol	Dimension Description	Dimension Units
v_y	Vertical Component of Fault Detector Induced Voltage	V
v_x	Horizontal Component of Fault Detector Induced Voltage	V
H_y	Vertical Component of Fault Detector Magnetic Field Intensity	A/m
H_x	Horizontal Component of Fault Detector Magnetic Field Intensity	A/m

The magnetic field intensity vector *H* shown in Figure 4.2 is comprised of the vertical and horizontal magnetic field intensity vectors H_y and H_x in Figure 4.6. This is illustrated in Figure 4.7.

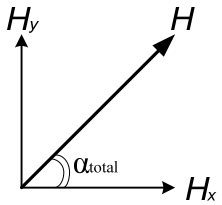

Figure 4.7: Magnetic Field Intensity Vector Components

Therefore, the vector *H* can be broken down into its two components using α, Ampère's law (Equation 3.7 where $r = \ell$), Equation 4.3, and Equation 4.4. The equations for the vertical and horizontal components are respectively given in Equation 4.5 and Equation 4.6.

$$H_y = H\sin(\alpha) = H\frac{\mathrm{d}}{\ell} = \left(\frac{i}{2\pi\ell}\right)\left(\frac{\mathrm{d}}{\ell}\right) = \frac{i\mathrm{d}}{2\pi\ell^2} \quad \text{(A/m)} \tag{4.5}$$

$$H_x = H\cos(\alpha) = H\frac{\mathrm{h}}{\ell} = \left(\frac{i}{2\pi\ell}\right)\left(\frac{\mathrm{h}}{\ell}\right) = \frac{i\mathrm{h}}{2\pi\ell^2} \quad \text{(A/m)} \tag{4.6}$$

The vertical and horizontal induced voltages v_y and v_x shown in Figure 4.5 can be solved using Faraday's law (Equation 3.3). Additionally, after establishing the relationship between magnetic field intensity (*H*) and magnetic flux density (*B*) in Equation 3.8 and Equation 3.9, Faraday's law can be rewritten as shown in Equation 4.7.

$$e = NA\frac{dB}{dt} = NA\frac{d}{dt}(\mu H) = \mu NA\frac{dH}{dt} \quad \text{(V)} \tag{4.7}$$

The vertical and horizontal induced voltages can then be solved using their respective magnetic field intensities and Equation 4.7 as respectively shown Equation 4.8 and Equation 4.9.

$$v_y = e = \mu NA\frac{dH_x}{dt} = \mu NA\frac{d}{dt}\left(\frac{i\mathrm{h}}{2\pi\ell^2}\right) = \frac{\mu NA\mathrm{h}}{2\pi\ell^2}\frac{di}{dt} \quad \text{(V)} \tag{4.8}$$

$$v_x = e = \mu NA\frac{dH_y}{dt} = \mu NA\frac{d}{dt}\left(\frac{i\mathrm{d}}{2\pi\ell^2}\right) = \frac{\mu NA\mathrm{d}}{2\pi\ell^2}\frac{di}{dt} \quad \text{(V)} \tag{4.9}$$

Using Equation 4.1, the derivative of remaining variable i is calculated (Equation 4.10).

$$\frac{di}{dt} = \frac{d(I_{MAX}\sin(\omega t))}{dt} = \omega I_{MAX}\cos(\omega t) \quad \text{(A)} \tag{4.10}$$

Substituting Equation 4.10 in Equation 4.8 and Equation 4.9 forms the new equations for the vertical and horizontal induced voltages given in Equation 4.11 and Equation 4.12.

$$v_y = \frac{\mu NA\mathrm{h}(\omega I_{MAX,y}\cos(\omega t))}{2\pi\ell^2} \quad \text{(V)} \tag{4.11}$$

$$v_x = \frac{\mu NA\mathrm{d}(\omega I_{MAX,x}\cos(\omega t))}{2\pi \ell^2} \quad \text{(V)} \tag{4.12}$$

Moreover, since the induced voltages have values that are characteristic of a wave as given in Equation 4.13, for fault detection it is necessary to convert the induced voltages to a root mean square (RMS) value as shown in Equation 4.14.

$$v(t) = V_{MAX}\sin(\omega t) \quad \text{(V)} \tag{4.13}$$

$$V_{RMS} = \frac{V_{MAX}}{\sqrt{2}} \quad \text{(V)} \tag{4.14}$$

Where for v_y:

$$V_{MAX,y} = \frac{\mu NA\mathrm{h}\omega I_{MAX,y}}{2\pi \ell^2} \quad \text{(V)} \tag{4.15}$$

And for v_x:

$$V_{MAX,x} = \frac{\mu NA\mathrm{d}\omega I_{MAX,x}}{2\pi \ell^2} \quad \text{(V)} \tag{4.16}$$

Therefore, the RMS values for the vertical and horizontal induced voltages are respectively given in Equation 4.17 and Equation 4.18.

$$V_{RMS,y} = \frac{\mu NA\mathrm{h}\omega I_{MAX,y}}{2\pi \ell^2\sqrt{2}} \quad \text{(V)} \tag{4.17}$$

$$V_{RMS,x} = \frac{\mu NA\mathrm{d}\omega I_{MAX,x}}{2\pi \ell^2\sqrt{2}} \quad \text{(V)} \tag{4.18}$$

The current I_{MAX} can be solved for after rearranging Equation 4.17 and Equation 4.18 as shown in Equation 4.19 and Equation 4.20.

$$I_{MAX,y} = \frac{2\pi \ell^2\sqrt{2}\,V_{RMS,y}}{\mu NA\mathrm{h}\omega} \quad \text{(A)} \tag{4.19}$$

$$I_{MAX,x} = \frac{2\pi \ell^2 \sqrt{2}\, V_{RMS,x}}{\mu N A \mathrm{d}\omega} \quad \text{(A)} \tag{4.20}$$

4.1.2 Three Phase System

The fault detector for a three phase design is illustrated in Figure 4.8.

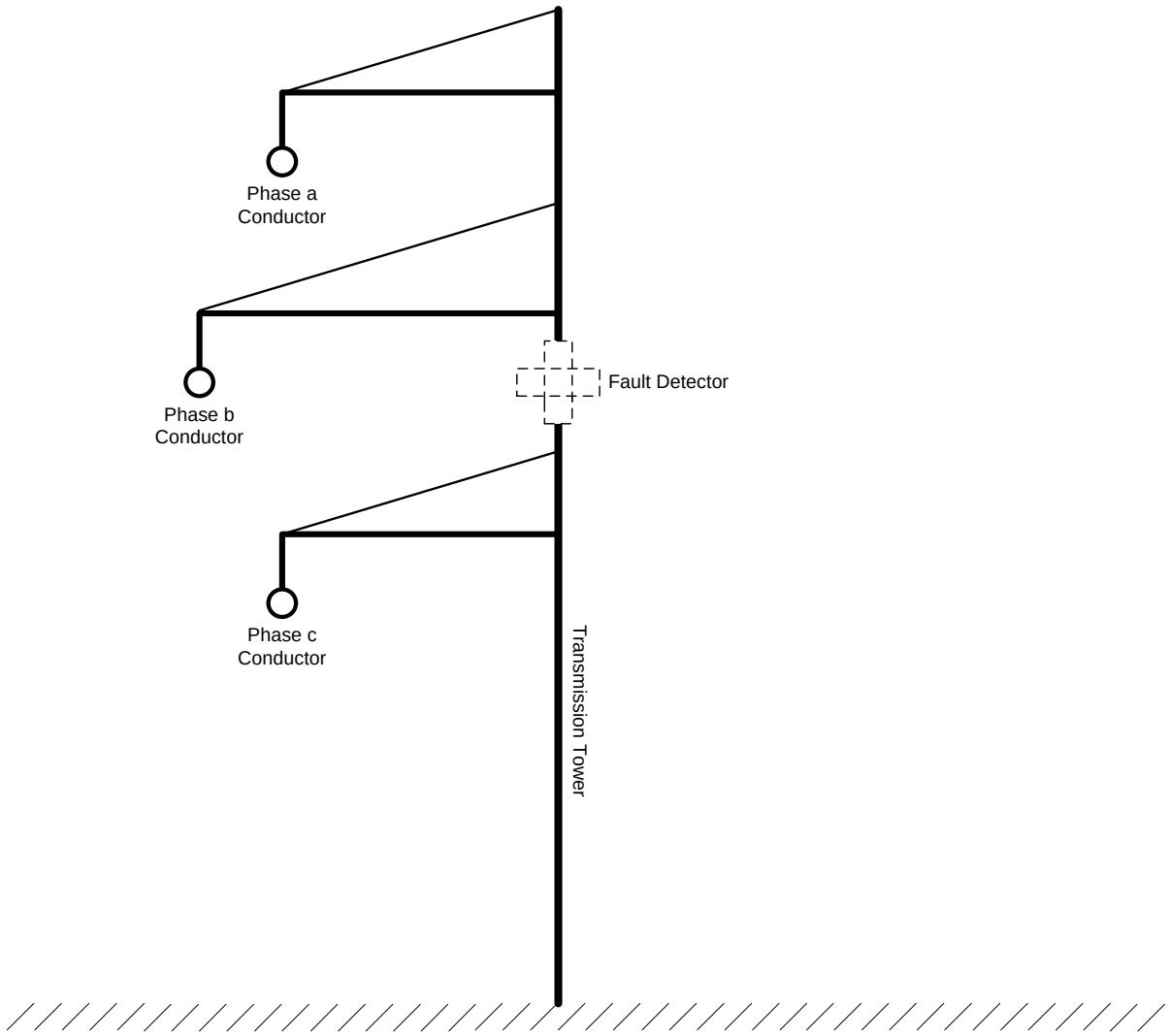

Figure 4.8: Three Phase Transmission Design

The design of Figure 4.8 can be defined with additional detail for the purpose of component measurement using trigonometry as shown in Figure 4.9. The dimensions of Figure 4.9 are defined in Table 4.3.

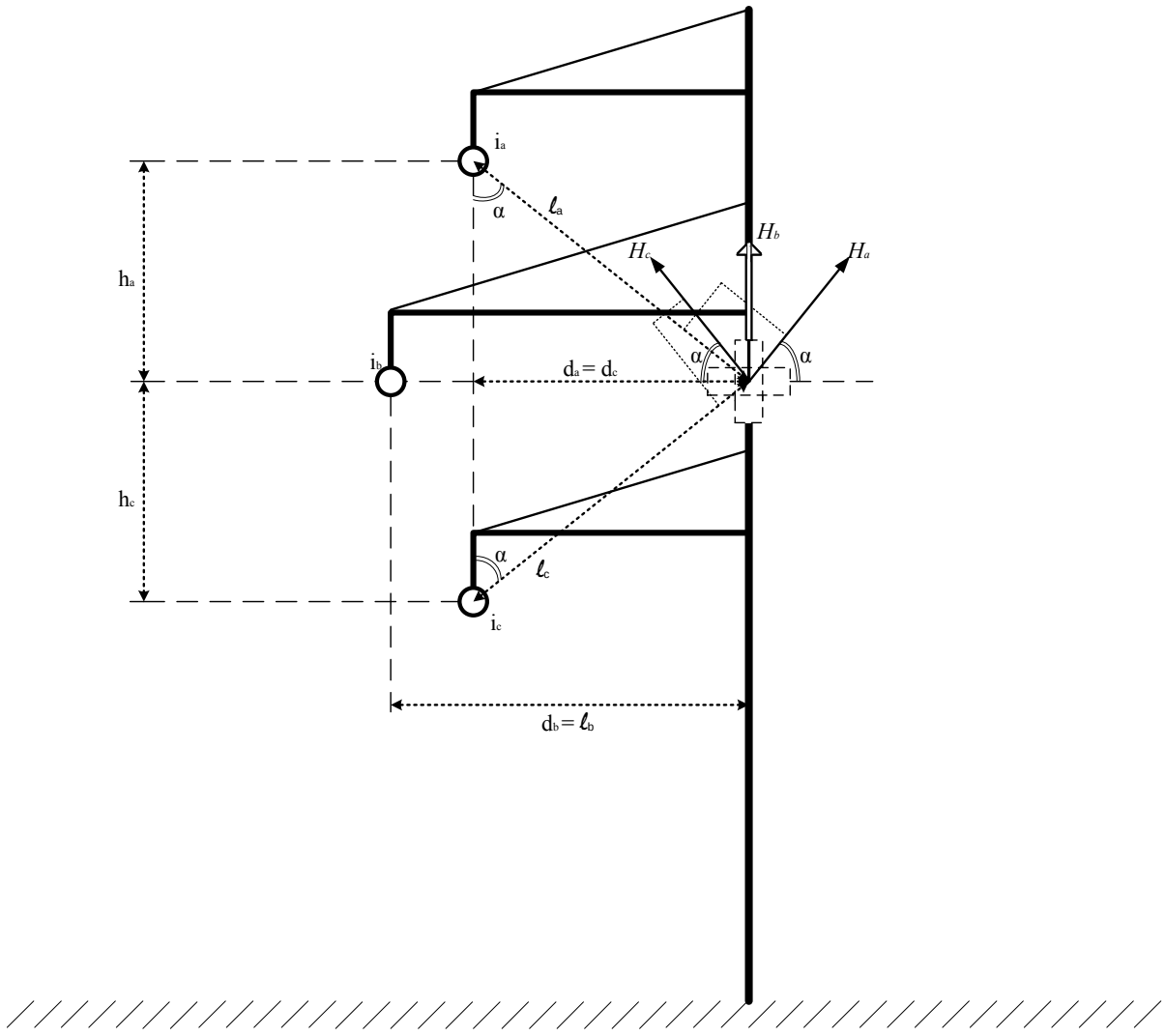

Figure 4.9: Dimensions of Three Phase Transmission Design

Table 4.3: Three Phase Transmission Design Dimensions Descriptions

Dimension Symbol	Dimension Description	Dimension Units
i_a	Current of Phase a Conductor	A
i_b	Current of Phase b Conductor	A
i_c	Current of Phase c Conductor	A
h_a	Height of Phase a Conductor from Fault Detector	m
h_c	Height of Phase c Conductor from Fault Detector	m
d_a	Horizontal Distance of Phase a Conductor from Fault Detector	m
d_b	Horizontal Distance of Phase b Conductor from Fault Detector	m
d_c	Horizontal Distance of Phase c Conductor from Fault Detector	m
ℓ_a	Length between Phase a Conductor and Fault Detector	m
ℓ_b	Length between Phase b Conductor and Fault Detector	m
ℓ_c	Length between Phase c Conductor and Fault Detector	m
α	Length Measurement ℓ Angle of Approach	Degree (°)
H_a	Phase a Magnetic Field Intensity	A/m
H_b	Phase b Magnetic Field Intensity	A/m
H_c	Phase c Magnetic Field Intensity	A/m

As defined in Equation 4.1, the current of the conductors have a sinusoidal value comprised of the maximum current (highest amplitude of the sin wave) I_{MAX} (A) and the frequency of the sin wave ω. However, in three phase systems three current waveforms are produced that are equal in magnitude and 120° out of phase to each other as illustrated in Figure 4.10. This produces a waveform similar to that of Figure 4.11.

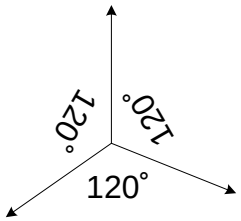

Figure 4.10: Phase Angles of Three Phase System

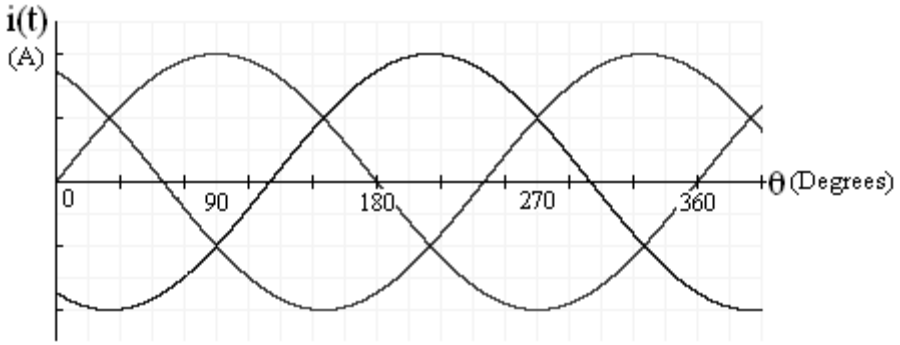

Figure 4.11: Waveform of Three Phase System

Due to the additional phases, the equation of the ac current wave with the phase angle φ takes the form of Equation 4.21 [7] where φ is the phase angle.

$$i = I_{MAX} \sin(\omega t + \varphi) \quad \text{(A)} \tag{4.21}$$

Similar to the single phase system, the length between the conductor and fault locator ℓ can be found using a variation of the Pythagorean theorem. The length for phase a and phase c are found using equations 4.22 and 4.23. Note that the length for phase b (ℓ_b) is equal to the distance d_b ad given in Equation 4.24.

$$\ell_a = \sqrt{h_a^{\,2} + d_a^{\,2}} \quad \text{(m)} \tag{4.22}$$

$$\ell_c = \sqrt{h_c^{\,2} + d_c^{\,2}} \quad \text{(m)} \tag{4.23}$$

$$\ell_b = \sqrt{h_b^{\,2} + d_b^{\,2}} = \sqrt{0^2 + d_b^{\,2}} = d_b \quad \text{(m)} \tag{4.24}$$

As discussed, the angle between the current in a conductor and its magnetic field intensity has a value of 90°, a right angle. It can again be assumed that the angles labeled α are equal due to the congruent triangles.

As shown in Figure 4.9, each of the three phases (phase a, phase b, and phase c) produce a magnetic field intensity vector (H_a, H_b, and H_c respectively). Each phase's magnetic field intensity vector is composed of a horizontal (H_{ax}, H_{bx}, and H_{cx}) and vertical (H_{ay}, H_{by}, and H_{cy}) component as shown in Figure 4.12 – Figure 4.14.

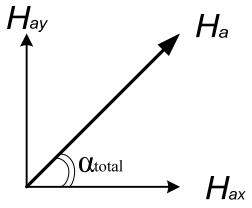

Figure 4.12: Phase a Magnetic Field Intensity

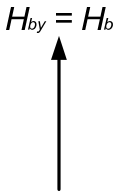

Figure 4.13: Phase b Magnetic Field Intensity

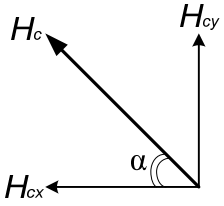

Figure 4.14: Phase c Magnetic Field Intensity

The total horizontal magnetic field intensity $H_{x,total}$, in a three phase system is the summation of all of the three phase's horizontal magnetic field intensities (H_{ax}, H_{bx}, and H_{cx}). Each of the horizontal field intensities can be determined using Ampère's law

(Equation 3.7 where $r = \ell$) and Equation 4.4 as shown in Equation 4.25, Equation 4.26, and Equation 4.27.

$$H_{ax} = H\cos(\alpha) = H\frac{\mathrm{h_a}}{\ell_a} = \left(\frac{i_a}{2\pi\ell_a}\right)\left(\frac{\mathrm{h_a}}{\ell_a}\right) = \frac{i_a \mathrm{h_a}}{2\pi\ell_a^{\,2}} \quad \text{(A/m)} \tag{4.25}$$

$$H_{bx} = H\cos(\alpha) = H\frac{\mathrm{h_b}}{\ell_b} = \left(\frac{i_b}{2\pi\ell_b}\right)\left(\frac{\mathrm{h_b}}{\ell_b}\right) = \frac{i_b \mathrm{h_b}}{2\pi\ell_b^{\,2}} \quad \text{(A/m)} \tag{4.26}$$

$$H_{cx} = H\cos(\alpha) = H\frac{\mathrm{h_c}}{\ell_c} = \left(\frac{i_c}{2\pi\ell_c}\right)\left(\frac{\mathrm{h_c}}{\ell_c}\right) = \frac{i_c \mathrm{h_c}}{2\pi\ell_c^{\,2}} \quad \text{(A/m)} \tag{4.27}$$

The total horizontal magnetic field intensity ($H_{\mathrm{x,total}}$) can then be found by adding Equation 4.25, Equation 4.26, and Equation 4.27 as shown in Equation 4.28.

$$H_{x,total} = H_{ax} + H_{bx} + H_{cx} = \left(\frac{i_a \mathrm{h_a}}{2\pi\ell_a^{\,2}}\right) + \left(\frac{i_b \mathrm{h_b}}{2\pi\ell_b^{\,2}}\right) + \left(\frac{i_c \mathrm{h_c}}{2\pi\ell_c^{\,2}}\right) \quad \text{(A/m)} \tag{4.28}$$

Similar to the total horizontal magnetic field intensity, the total vertical magnetic field intensity ($H_{\mathrm{y,total}}$) in a three phase system is the summation of all of the three phase's vertical magnetic field intensities (H_{ay}, H_{by}, and H_{cy}). Each of the vertical field intensities can be determined using Ampère's law (Equation 3.7 where $r = \ell$) and Equation 4.3 as shown in Equation 4.29, Equation 4.30, and Equation 4.31.

$$H_{ay} = H\sin(\alpha) = H\frac{\mathrm{d_a}}{\ell_a} = \left(\frac{i_a}{2\pi\ell_a}\right)\left(\frac{\mathrm{d_a}}{\ell_a}\right) = \frac{i_a \mathrm{d_a}}{2\pi\ell_a^{\,2}} \quad \text{(A/m)} \tag{4.29}$$

$$H_{by} = H\sin(\alpha) = H\frac{\mathrm{d_b}}{\ell_b} = \left(\frac{i_b}{2\pi\ell_b}\right)\left(\frac{\mathrm{d_b}}{\ell_b}\right) = \frac{i_b \mathrm{d_b}}{2\pi\ell_b^{\,2}} \quad \text{(A/m)} \tag{4.30}$$

$$H_{cy} = H\sin(\alpha) = H\frac{\mathrm{d_c}}{\ell_c} = \left(\frac{i_c}{2\pi\ell_c}\right)\left(\frac{\mathrm{d_c}}{\ell_c}\right) = \frac{i_c \mathrm{d_c}}{2\pi\ell_c^{\,2}} \quad \text{(A/m)} \tag{4.31}$$

The total vertical magnetic field intensity ($H_{y,total}$) can then be found by adding Equation 4.29, Equation 4.30, and Equation 4.31 as shown in Equation 4.32.

$$H_{y,total} = H_{ay} + H_{by} + H_{cy} = \left(\frac{i_a \mathrm{d_a}}{2\pi \ell_a^{\,2}}\right) + \left(\frac{i_b \mathrm{d_b}}{2\pi \ell_b^{\,2}}\right) + \left(\frac{i_c \mathrm{d_c}}{2\pi \ell_c^{\,2}}\right) \quad \text{(A/m)} \qquad (4.32)$$

The total horizontal and vertical magnetic field intensities are used to find the total magnetic field intensity vector (H_{total}), as illustrated in Figure 4.15. The vector (H_{abc}) and its angle (α_{total}) can be found using Equation 4.33 and Equation 4.34.

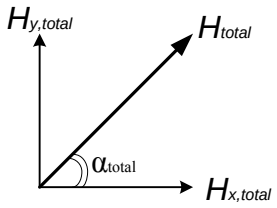

Figure 4.15: Three Phase Total Magnetic Field Intensity

$$H_{total} = \sqrt{H_{x,total}^{\,2} + H_{y,total}^{\,2}} \quad \text{(A/m)} \qquad (4.33)$$

$$\tan(\alpha_{total}) = \frac{H_{y,total}}{H_{x,total}} \quad (^\circ) \qquad (4.34)$$

In determining the three phase system's induced voltages it is found that the horizontal induced voltage v_x can be solved using Faraday's law as given in Equation 4.7. This solution is shown in Equation 4.35. The vertical induced voltage v_y is solved in the same way as shown in Equation 4.36.

$$v_x = e = \mu NA \frac{dH_{y,total}}{dt} = \mu NA \frac{d}{dt}\left(\left(\frac{i_a \mathrm{d_a}}{2\pi \ell_a^{\,2}}\right) + \left(\frac{i_b \mathrm{d_b}}{2\pi \ell_b^{\,2}}\right) + \left(\frac{i_c \mathrm{d_c}}{2\pi \ell_c^{\,2}}\right)\right) \quad \text{(V)} \qquad (4.35)$$

$$v_y = e = \mu NA \frac{dH_{x,total}}{dt} = \mu NA \frac{d}{dt}\left(\left(\frac{i_a \mathrm{h_a}}{2\pi \ell_a^{\,2}}\right) + \left(\frac{i_b \mathrm{h_b}}{2\pi \ell_b^{\,2}}\right) + \left(\frac{i_c \mathrm{h_c}}{2\pi \ell_c^{\,2}}\right)\right) \quad \text{(V)} \qquad (4.36)$$

4.2 Fault Locator

The fault location scheme in a transmission system is illustrated in Figure 4.16 with its components described in Table 4.4. This method applies to single phase and three phase systems.

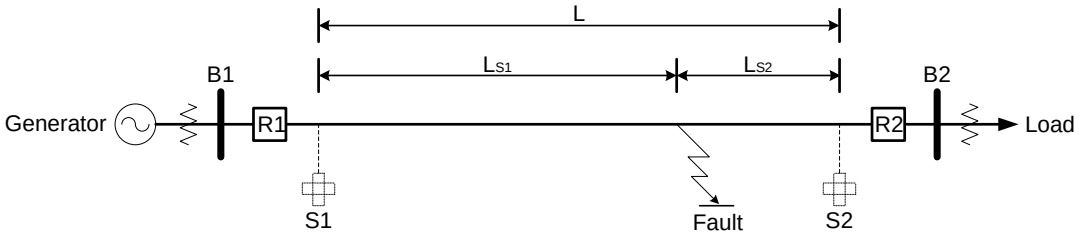

Figure 4.16: Fault Location Scheme in a Transmission System

Table 4.4: Components in Fault Location Scheme

Component Symbol	Component Description
B1	Bus 1 – Generator
B2	Bus 2 – Load
R1	Protective Relay for B1
R2	Protective Relay for B2
S1	Fault Locator Station for B1
S2	Fault Locator Station for B2
L	Length between Fault Locator Stations (m)
L_{S1}	Length between S1 and Fault Location (m)
L_{S2}	Length between S2 and Fault Location (m)

Using the transmission system diagram in Figure 4.16, the time at which fault locators S1 and S2 detect a fault can be described as:

t_{S1} = Difference in time between fault origin and fault detection at S1 (s)

t_{S2} = Difference in time between fault origin and fault detection at S2 (s)

The detection time of the fault locator that first detects a fault can be considered as the initial detection time, t_0. Additionally, the detection time of the fault locator to detect a fault after

the initial detection can be defined as t_x. The difference in detection time (Δt) between t_0 and t_x is given in Equation 4.37.

$$\Delta t = t_x - t_0 \quad \text{(s)} \tag{4.37}$$

Using a reduced form of the Telegrapher's equation (Equation 4.38 where L=Line Inductance and C=Line Capacitance), it is possible to find the total time for a signal to travel a transmission line. In this equation, the value for the traveling speed of a signal (c) is equal to a little less than the speed of light (299.79 x 10^6 m/s) which will be used as this variable's value for simplification purposes.

$$c = \frac{1}{\sqrt{LC}} \quad \text{(m/s)} \tag{4.38}$$

Assuming that the line length L is known, the time for a signal to travel the length of the transmission line (t_{total}) is given in Equation 4.39.

$$t_{total} = \frac{L}{c} \quad \text{(s)} \tag{4.39}$$

The values for t_{S1} and t_{S2} can then be calculated using the total time t_{total}. The difference between t_{total} and Δt divided by two (due to the two components it contributes to) equals the amount of time the signal was traveling before it was initially detected at t_0. This amount of time prior to detection is referred to as Δt_i is shown in Equation 4.40. Therefore, the amount of time between fault generation and fault location at S1 equals the difference in detection time (Δt) between t_0 and t_x in addition to the initial time Δt_i (Equation 4.41). The amount of time between fault generation and fault location at S2 equals initial time Δt_i (Equation 4.42).

$$\Delta t_i = \frac{t_{total} - \Delta t}{2} \quad \text{(s)} \tag{4.40}$$

$$t_{S1} = \Delta t + \Delta t_i \quad \text{(s)} \tag{4.41}$$

$$t_{S2} = \Delta t_i \quad \text{(s)} \tag{4.42}$$

To find the location of the fault a simple percentage equality between time and distance is calculated. The percent of time between fault generation and fault detection at a fault location station (t_S) divided by the total time for a signal to travel the line (t_{total}) is equal to the percentage of the total line length (L) where the fault is located from the station (L_S). This relationship is shown in Equation 4.43.

$$\frac{t_S}{t_{total}} = \frac{L_S}{L} \tag{4.43}$$

Solving for L_S:

$$L_S = \frac{L\,t_S}{t_{total}} \quad \text{(m)} \tag{4.44}$$

The distance between the fault origin and the fault locators S1 and S2 can then solved as shown in Equation 4.45 and Equation 4.46.

$$L_{S1} = \frac{L\,t_{S1}}{t_{total}} \quad \text{(m)} \tag{4.45}$$

$$L_{S2} = \frac{L\,t_{S2}}{t_{total}} \quad \text{(m)} \tag{4.46}$$

5 System Simulation and Analysis

This sections presents simulation studies of the fault detector for single phase and three phase systems and the fault locator. The results of the simulations conducted are analyzed for evaluation of the system's performance.

5.1 Fault Detector

The simulation and analysis of the fault detector is conducted for two systems, a single phase and three phase system. Each system is modeled after the proposed physical arrangement with values assigned to parameters that are assumed to be known.

5.1.1 Single Phase System

The single phase system is based on the model shown in Figure 4.2. For the purpose of simulation, the current (*i*), height (h), and distance (d) parameters as described in Table 4.2 are defined as shown in Figure 5.1 and Table 5.1.

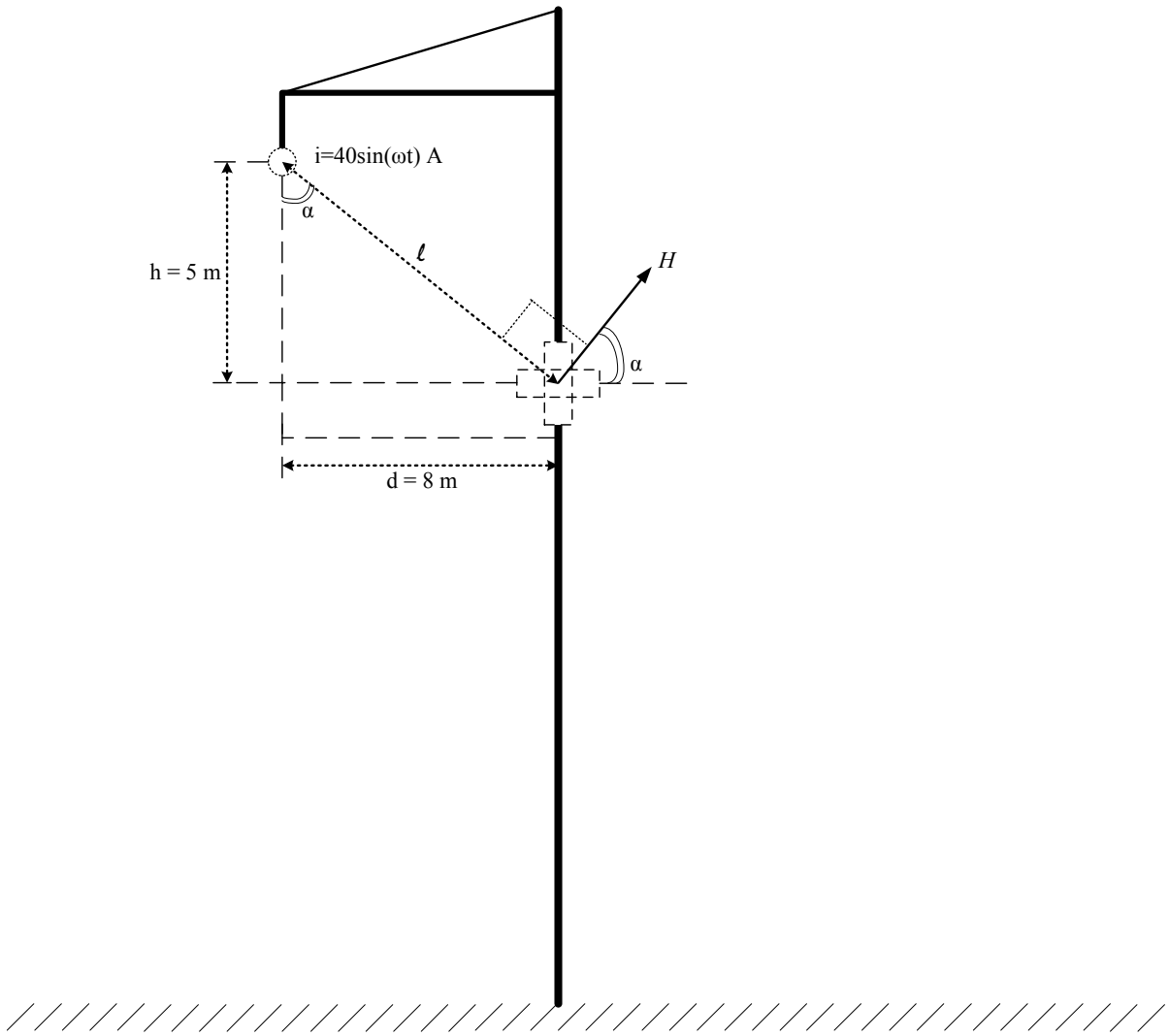

Figure 5.1: Single Phase Transmission Design with Parameters

Table 5.1: Single Phase Transmission Design Parameter Descriptions

Dimension Symbol	Dimension Value	Dimension Units
i	$i = 40\sin(\omega t)$	A
h	h = 5	m
d	d = 8	m

The detection of a fault occurs when the current at the detector equals zero. The root mean square (RMS) of the voltage as a periodic function (Equation 4.15 and Equation 4.16) is equal to the RMS of one period of the function. Therefore, if the current of the system is

equal to zero for one period of the voltage function, the RMS of the voltage will equal zero as shown in Equation 5.1. If the current is a value other than zero, the voltage will be equal to a positive number greater than zero that corresponds to the current input. Additionally, the detection of a fault depends on both the vertical and horizontal induced voltages. The detection of a fault occurs when both voltages have a RMS value of zero.

$$V_{RMS} = \frac{\mu NA\mathrm{h}\omega I_{MAX}}{2\pi \ell^2 \sqrt{2}} = \frac{\mu NA\mathrm{h}\omega(0)}{2\pi \ell^2 \sqrt{2}} = 0 \quad \text{(V)} \tag{5.1}$$

The single phase fault detector can be simulated by a graph of the vertical and horizontal RMS voltages with corresponding equations shown in Equation 5.2 and Equation 5.3 (as given by Equation 4.17 and Equation 4.18)

$$V_{RMS,y} = \frac{\mu NA\mathrm{h}\omega I_{MAX,y}}{2\pi \ell^2 \sqrt{2}} \quad \text{(V)} \tag{5.2}$$

$$V_{RMS,x} = \frac{\mu NA\mathrm{d}\omega I_{MAX,x}}{2\pi \ell^2 \sqrt{2}} \quad \text{(V)} \tag{5.3}$$

To evaluate these voltages, additional parameters including μ, N, A, ω, I_{MAX}, and ℓ must be either assigned a value or determined. Variables μ, N, A, ω, and I_{MAX} are assumed to be known; therefore values as given in Table 5.2 will be assigned. However, the surface area A must be calculated. Assuming that the radius, r, is equal to 0.5m, the surface area can be calculated as indicated in Equation 5.4. Additionally, the length between the conductor and fault locator, ℓ, must be determined using Equation 4.2 as shown in Equation 5.5.

Table 5.2: Variable Assignment for Single Phase Induced Voltage Equation

Dimension Symbol	Dimension Value	Dimension Units
r	$r = 0.5$	m
μ	$\mu = \mu_0 = 4\pi \times 10^{-7}$	Wb/Am
N	$N = 1000$	turns
ω	$\omega = 2\pi$	rad/s
I_{MAX}	$0 \le I_{MAX} \le 40$	A

$$A = \pi r^2 = \pi(0.5\text{m})^2 = 7.854 \times 10^{-1} \quad (\text{m}^2) \tag{5.4}$$

$$\ell = \sqrt{\text{h}^2 + \text{d}^2} = \sqrt{5\text{m}^2 + 8\text{m}^2} = 9.434 \quad (\text{m}) \tag{5.5}$$

The equations for vertical and horizontal RMS voltages can then be written as shown in Equation 5.6 and Equation 5.7 and graphed for simulation. The resulting graph is shown in Figure 5.2.

$$V_{RMS,y} = \frac{(4\pi \times 10^{-7}\ \text{Wb/Am})(1000\text{turns})(\pi(0.5\text{m})^2)(5\text{m})(2\pi\ \text{rad/s})(\text{I}_{\text{MAX}}\text{A})}{2\pi\left(\left(\sqrt{5^2 + 8^2}\right)\text{m}\right)^2\sqrt{2}} \quad (\text{V}) \tag{5.6}$$

$$V_{RMS,x} = \frac{(4\pi \times 10^{-7}\ \text{Wb/Am})(1000\text{turns})(\pi(0.5\text{m})^2)(8\text{m})(2\pi\ \text{rad/s})(\text{I}_{\text{MAX}}\text{A})}{2\pi\left(\left(\sqrt{5^2 + 8^2}\right)\text{m}\right)^2\sqrt{2}} \quad (\text{V}) \tag{5.7}$$

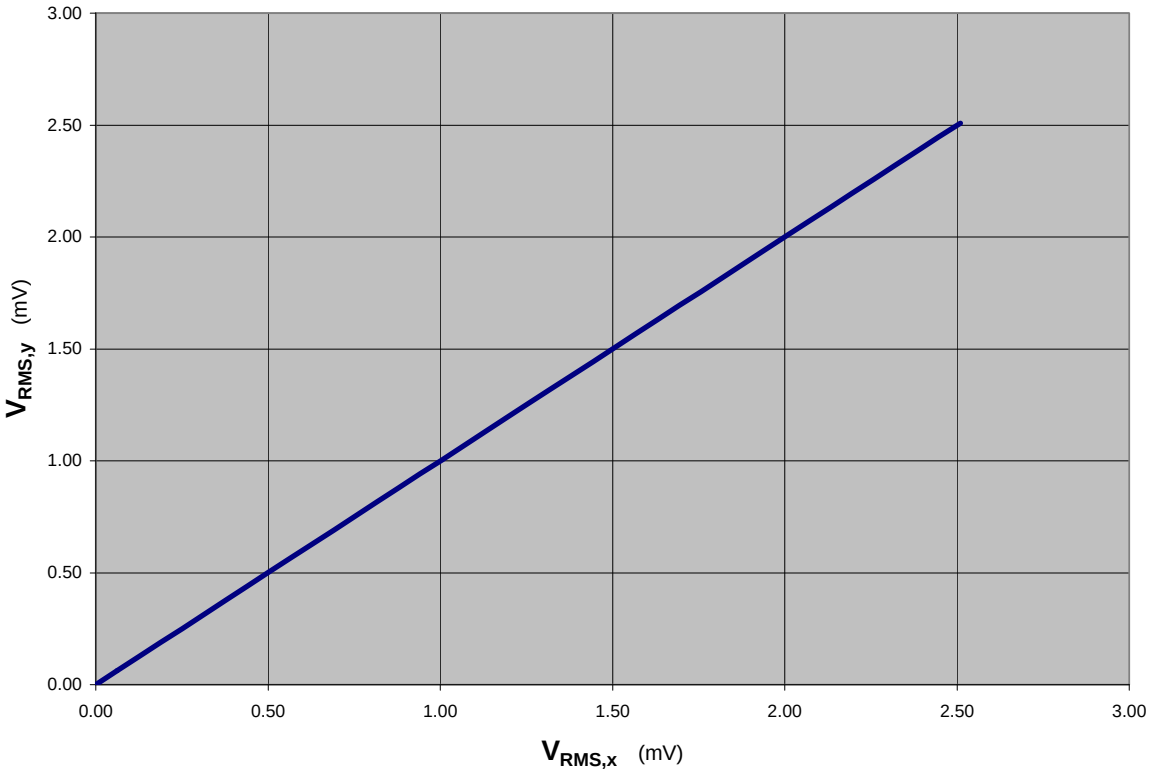

Figure 5.2: Graph of Single Phase Vertical and Horizontal RMS Voltages

The graph shown in Figure 5.2 illustrates the desired performance of the fault detector. More specifically, the vertical and horizontal RMS voltages vary according to the increase in I_{MAX} as it increments through its range of $0A \leq I_{MAX} \leq 40A$ (refer to Appendix C for specific values). For any value of $I_{MAX} > 0A$, both the vertical and horizontal RMS voltages equal a value greater than 0V. When $I_{MAX} = 0A$, the vertical and horizontal RMS voltages both equal 0V. This results in a line with a positive slope and a (x, y) intercept of (0.00mV, 0.00mV) when $I_{MAX} = 0A$.

The intercept of (0.00mV, 0.00mV) correctly models the point where the vertical and horizontal RMS voltages both equal zero which, as previously mentioned, indicates the existence of a fault. Therefore, if the fault detector input I_{MAX} in Equation 5.6 and Equation

5.7 results in 0V for both RMS voltages, the existence of a fault in a transmission line is assumed and detected.

This method can also be modeled on PSpice for analysis. The magnetic field intensity at a sensor is a function of the a conductor's current in a transmission system. The vertical and horizontal components of the magnetic field intensity of Figure 5.1 are calculated as shown in Equation 5.8 and Equation 5.9.

$$H_y = H\sin(\alpha) = H\frac{\mathrm{d}}{\ell} = \left(\frac{i}{2\pi\ell}\right)\left(\frac{\mathrm{d}}{\ell}\right) = \frac{i\mathrm{d}}{2\pi\ell^2} = \frac{i(8)}{2\pi(9.434\mathrm{m})^2} = i(0.014306) \quad \text{(A/m)} \quad (5.8)$$

$$H_x = H\cos(\alpha) = H\frac{\mathrm{h}}{\ell} = \left(\frac{i}{2\pi\ell}\right)\left(\frac{\mathrm{h}}{\ell}\right) = \frac{i\mathrm{h}}{2\pi\ell^2} = \frac{i(5\mathrm{m})}{2\pi(9.434\mathrm{m})^2} = i(0.008941) \quad \text{(A/m)} \quad (5.9)$$

The vertical and horizontal magnetic field components can then be related to the induced voltage by Faraday's law (Equation 3.3) and Equation 4.7, Equation 4.8, and Equation 4.9.

The PSpice single phase transmission line for simulation with no fault is shown in Figure 5.3. A graph of Figure 5.3's magnetic field intensities as calculated in Equation 5.8 and Equation 5.9 is shown in Figure 5.4.

Figure 5.3: PSpice Single Phase Transmission Schematic

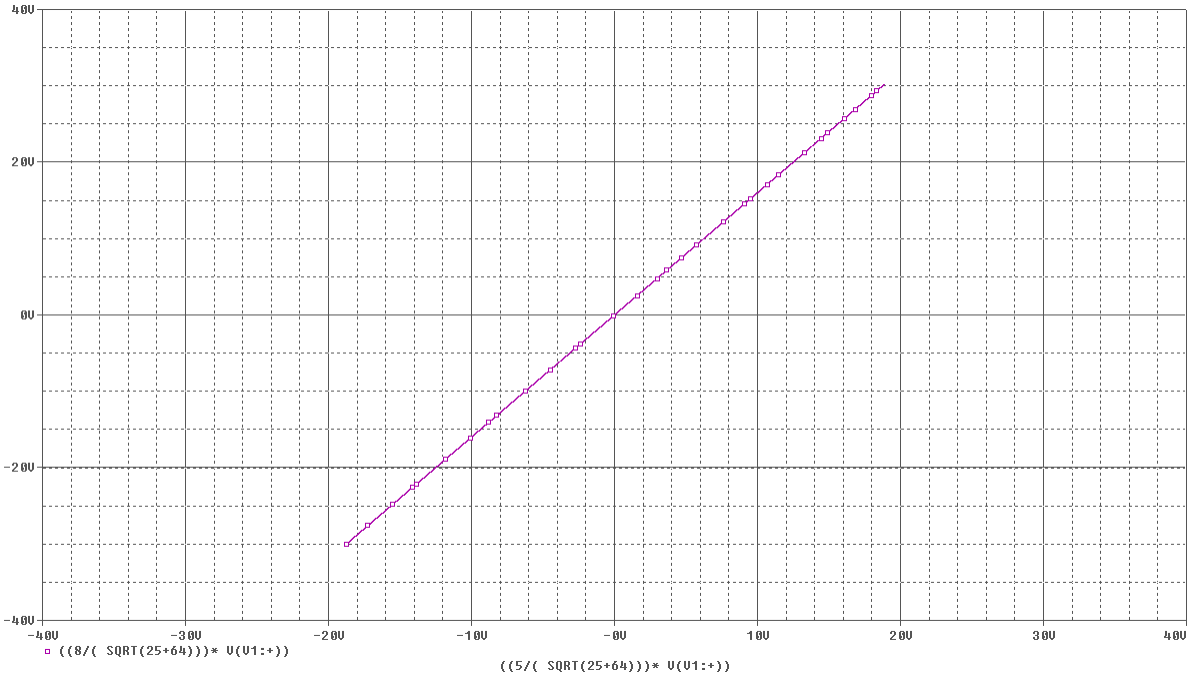

Figure 5.4: PSpice Singe Phase Transmission Magnetic Field Intensity

If a fault were to occur on the transmission line of Figure 5.3 as shown in Figure 5.5, it would result in a change in the magnetic field intensity as shown in Figure 5.6.

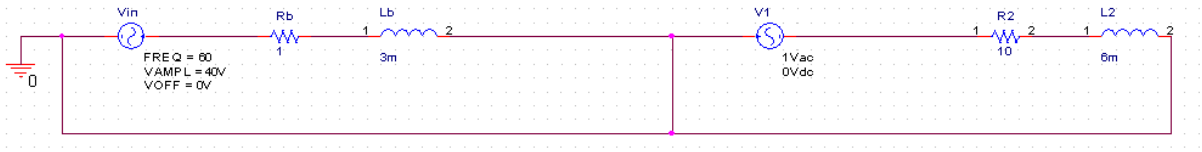

Figure 5.5: PSpice Single Phase Transmission Fault Schematic

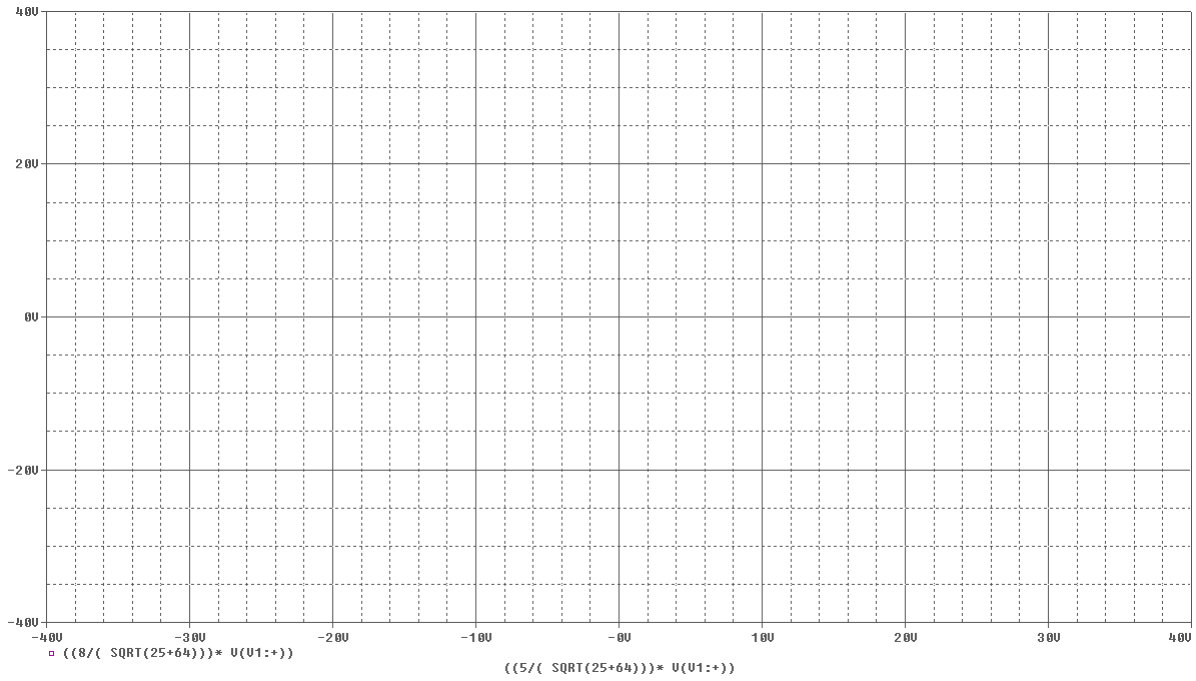

Figure 5.6: PSpice Singe Phase Transmission Fault Magnetic Field Intensity

The comparison of the plot in Figure 5.4 and Figure 5.6 indicates that when a fault occurs, the magnetic field intensity, a component of the induced voltage, equals zero. Therefore, if the induced voltage at the fault sensor observed a magnetic field intensity of zero, it would be an indication of a fault on a transmission line.

The above analysis of the fault detector simulation for a single phase system indicates the successful detection of a fault on the transmission line. The calculations of the applicable

equations result in values that when modeled by graphs, correctly indicate the system's ability to detect a fault when there is an absence of current in the transmission line.

5.1.2 Three Phase System

A more complicated fault detector simulation is that of a three phase system based on the model shown in Figure 4.9. To simulate this system, the parameters of the phase angles (φ_a, φ_b, φ_c), currents (i_a, i_b, i_c), heights (h_a, h_b, h_c), and distances (d_a, d_b, d_c) as described in Table 4.3 are defined as shown in Figure 5.7 and Table 5.3. Note that the location of the bottom conductor (phase c) has a negative H_{cx} vector component.

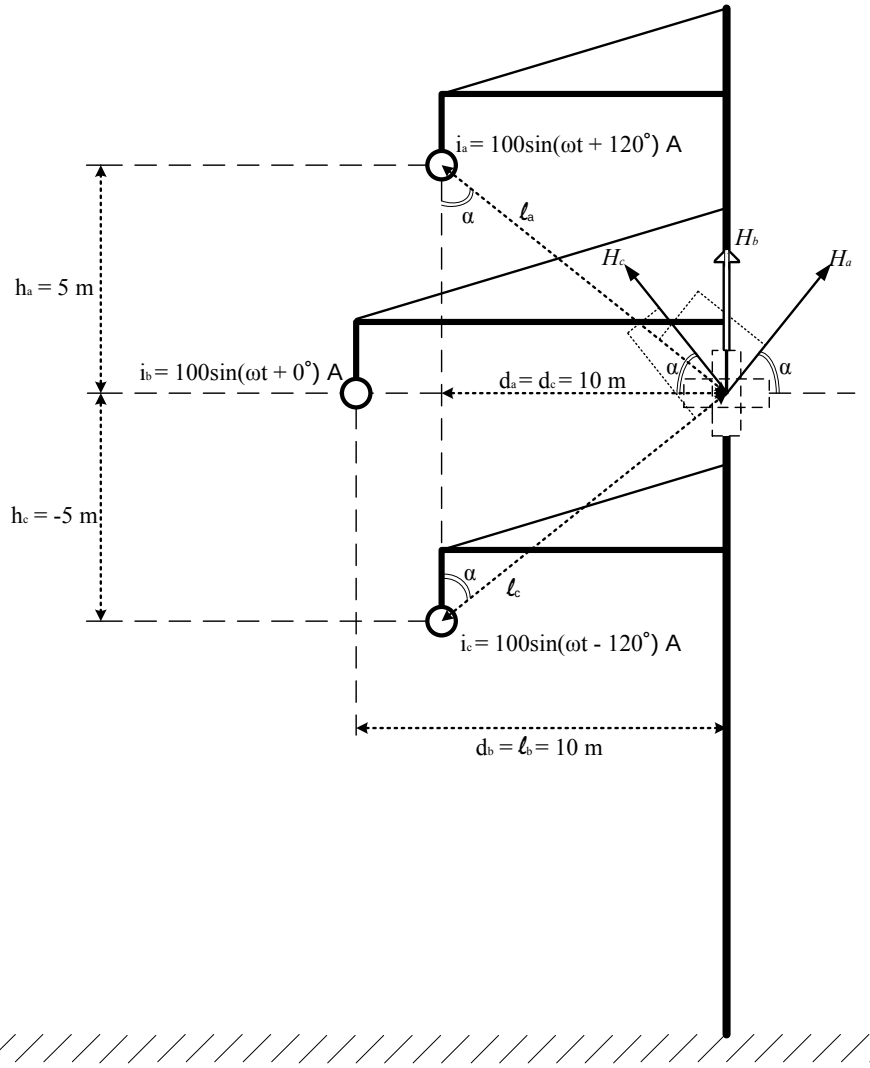

Figure 5.7: Three Phase Transmission Design with Parameters

Table 5.3: Three Phase Transmission Design Parameter Descriptions

Dimension Symbol	Dimension Value	Dimension Units
φ_a	$\varphi_a = 120$	Degrees (°)
φ_b	$\varphi_b = 0$	Degrees (°)
φ_c	$\varphi_c = -120$	Degrees (°)
i_a	$i_a = 100\sin(\omega t + 120°)$	A
i_b	$i_b = 100\sin(\omega t + 0°)$	A
i_c	$i_c = 100\sin(\omega t - 120°)$	A
h_a	$h_a = 5$	m
h_b	$h_b = 0$	m
h_c	$h_c = -5$	m
d_a	$d_a = 8$	m
d_b	$d_b = 10$	m
d_c	$d_c = 8$	m

Using the values given in Table 5.3 and Equation 4.2, the ℓ component for phase a, phase b, and phase c can be calculated as shown in Equation 5.10, Equation 5.11, and Equation 5.12.

$$\ell_a = \sqrt{h_a^{\,2} + d_a^{\,2}} = \sqrt{5m^2 + 8m^2} = 9.434 \quad \text{(m)} \tag{5.10}$$

$$\ell_b = \sqrt{h_b^{\,2} + d_b^{\,2}} = \sqrt{0m^2 + 10m^2} = 10 \quad \text{(m)} \tag{5.11}$$

$$\ell_c = \sqrt{h_c^{\,2} + d_c^{\,2}} = \sqrt{-5m^2 + 8m^2} = 9.434 \quad \text{(m)} \tag{5.12}$$

The phase a, phase b, and phase c horizontal and vertical magnetic field intensities as given in Equation 4.25. Equation 4.26, and Equation 4.27, Equation 4.29, Equation 4.30, and Equation 4.31 can be solved as respectively shown in Equation 5.13, Equation 5.14, Equation 5.15, Equation 5.16, Equation 5.17, and Equation 5.18.

$$H_{ax} = H\cos(\alpha) = H\frac{\mathrm{h_a}}{\ell_a} = \left(\frac{i_a}{2\pi\ell_a}\right)\left(\frac{\mathrm{h_a}}{\ell_a}\right) = \frac{i_a\mathrm{h_a}}{2\pi\ell_a{}^2} = \frac{i_a(5\mathrm{m})}{2\pi(9.434\mathrm{m})^2} = i_a(0.008941)\,(\mathrm{A/m}) \quad (5.13)$$

$$H_{bx} = H\cos(\alpha) = H\frac{\mathrm{h_b}}{\ell_b} = \left(\frac{i_b}{2\pi\ell_b}\right)\left(\frac{\mathrm{h_b}}{\ell_b}\right) = \frac{i_b\mathrm{h_b}}{2\pi\ell_b{}^2} = \frac{i_b(0\mathrm{m})}{2\pi(10\mathrm{m})^2} = i_b(0) \quad (\mathrm{A/m}) \quad (5.14)$$

$$H_{cx} = H\cos(\alpha) = H\frac{\mathrm{h_c}}{\ell_c} = \left(\frac{i_c}{2\pi\ell_c}\right)\left(\frac{\mathrm{h_c}}{\ell_c}\right) = \frac{i_c\mathrm{h_c}}{2\pi\ell_c{}^2} = \frac{i_c(-5\mathrm{m})}{2\pi(9.434\mathrm{h})^2} = i_c(-0.008941)\,(\mathrm{A/m}) \quad (5.15)$$

$$H_{ay} = H\sin(\alpha) = H\frac{\mathrm{d_a}}{\ell_a} = \left(\frac{i_a}{2\pi\ell_a}\right)\left(\frac{\mathrm{d_a}}{\ell_a}\right) = \frac{i_a\mathrm{d_a}}{2\pi\ell_a{}^2} = \frac{i_a(8\mathrm{m})}{2\pi(9.434\mathrm{m})^2} = i_a(0.014306)\,(\mathrm{A/m}) \quad (5.16)$$

$$H_{by} = H\sin(\alpha) = H\frac{\mathrm{d_b}}{\ell_b} = \left(\frac{i_b}{2\pi\ell_b}\right)\left(\frac{\mathrm{d_b}}{\ell_b}\right) = \frac{i_b\mathrm{d_b}}{2\pi\ell_b{}^2} = \frac{i_b(10\mathrm{m})}{2\pi(10\mathrm{m})^2} = i_b(0.015915) \quad (\mathrm{A/m}) \quad (5.17)$$

$$H_{cy} = H\sin(\alpha) = H\frac{\mathrm{d_c}}{\ell_c} = \left(\frac{i_c}{2\pi\ell_c}\right)\left(\frac{\mathrm{d_c}}{\ell_c}\right) = \frac{i_c\mathrm{d_c}}{2\pi\ell_c{}^2} = \frac{i_c(8\mathrm{m})}{2\pi(9.434\mathrm{m})^2} = i_c(0.014306)\,(\mathrm{A/m}) \quad (5.18)$$

The total horizontal and vertical magnetic fields can then be solved using Equation 4.28 and Equation 4.32 as shown in Equation 5.19 and Equation 5.20.

$$\begin{aligned} H_{x,total} &= H_{ax} + H_{bx} + H_{cx} \\ &= \left(\frac{i_a\mathrm{h_a}}{2\pi\ell_a{}^2}\right) + \left(\frac{i_b\mathrm{h_b}}{2\pi\ell_b{}^2}\right) + \left(\frac{i_c\mathrm{h_c}}{2\pi\ell_c{}^2}\right) \\ &= i_a(0.008941) + i_b(0) + i_c(-0.008941) \quad (\mathrm{A/m}) \end{aligned} \quad (5.19)$$

$$\begin{aligned} H_{y,total} &= H_{ay} + H_{by} + H_{cy} \\ &= \left(\frac{i_a\mathrm{d_a}}{2\pi\ell_a{}^2}\right) + \left(\frac{i_b\mathrm{d_b}}{2\pi\ell_b{}^2}\right) + \left(\frac{i_c\mathrm{d_c}}{2\pi\ell_c{}^2}\right) \\ &= i_a(0.014306) + i_b(0.015915) + i_c(0.014306) \quad (\mathrm{A/m}) \end{aligned} \quad (5.20)$$

Using Equation 5.19 and Equation 5.20, the magnetic field intensity can be simulated and graphed using PSpice. The schematic for a three phase system modeled in PSpice is shown in Figure 5.8.

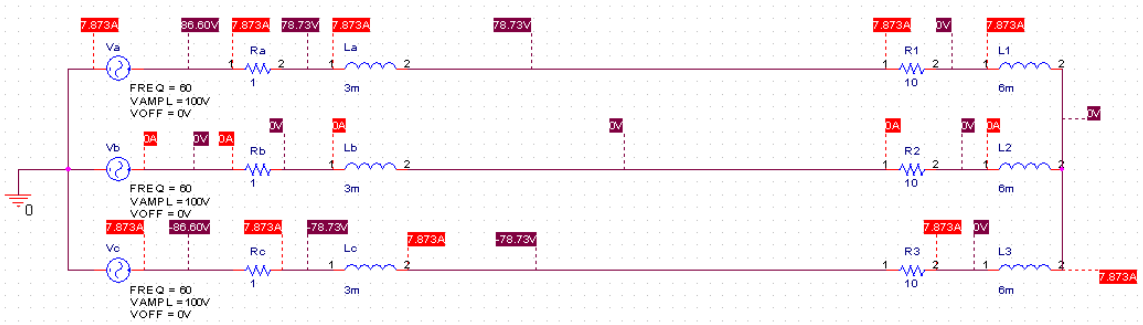

Figure 5.8: PSpice Three Phase Transmission Schematic

In Figure 5.8 there are no faults in the system, therefore is considered the neutral case. Using this case, and Equation 5.19 and Equation 5.20 the neutral graphs for phase a, phase b, and phase c magnetic field intensities can be simulated as shown in Figure 5.9, Figure 5.10, and Figure 5.11 respectively. These graphs isolate each phase's magnetic field intensity. Figure 5.12 again simulates the case of Figure 5.8, however it shows the total horizontal and vertical magnetic field intensities of all three phases.

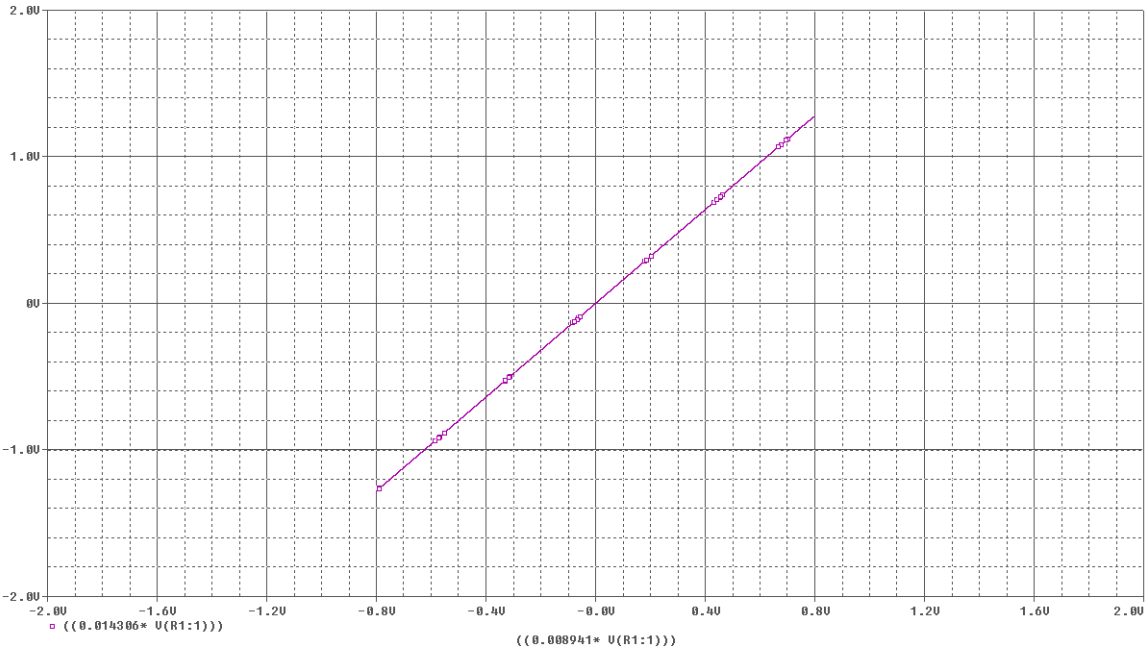

Figure 5.9: PSpice Three Phase Transmission H_a Magnetic Field Intensity

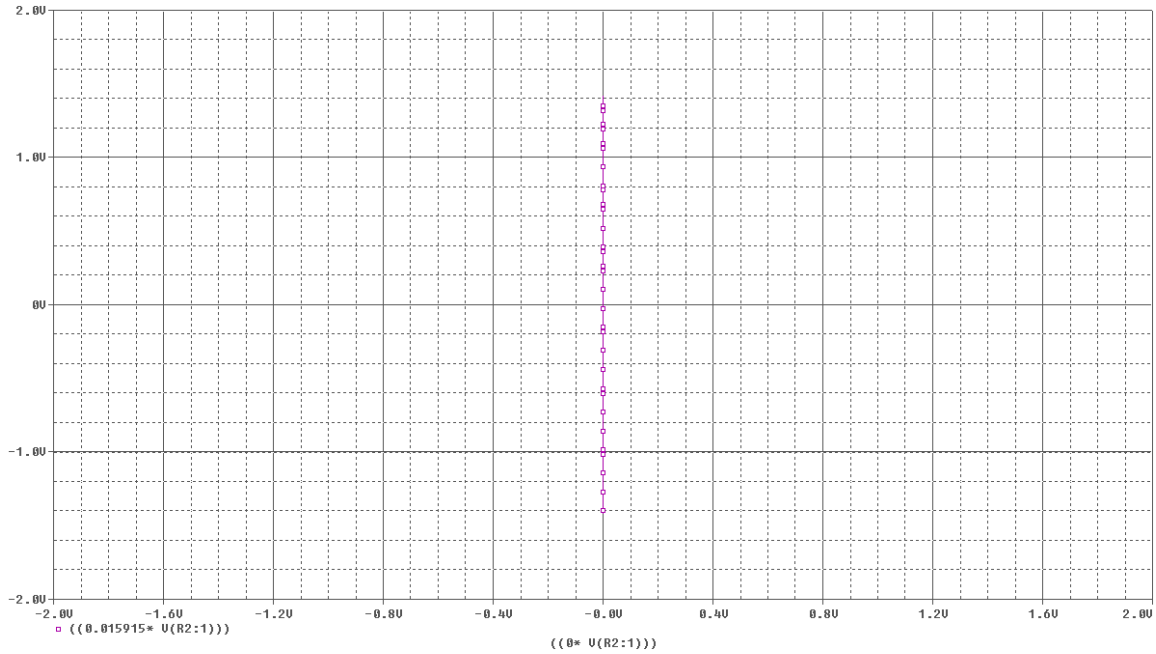

Figure 5.10: PSpice Three Phase Transmission H_b Magnetic Field Intensity

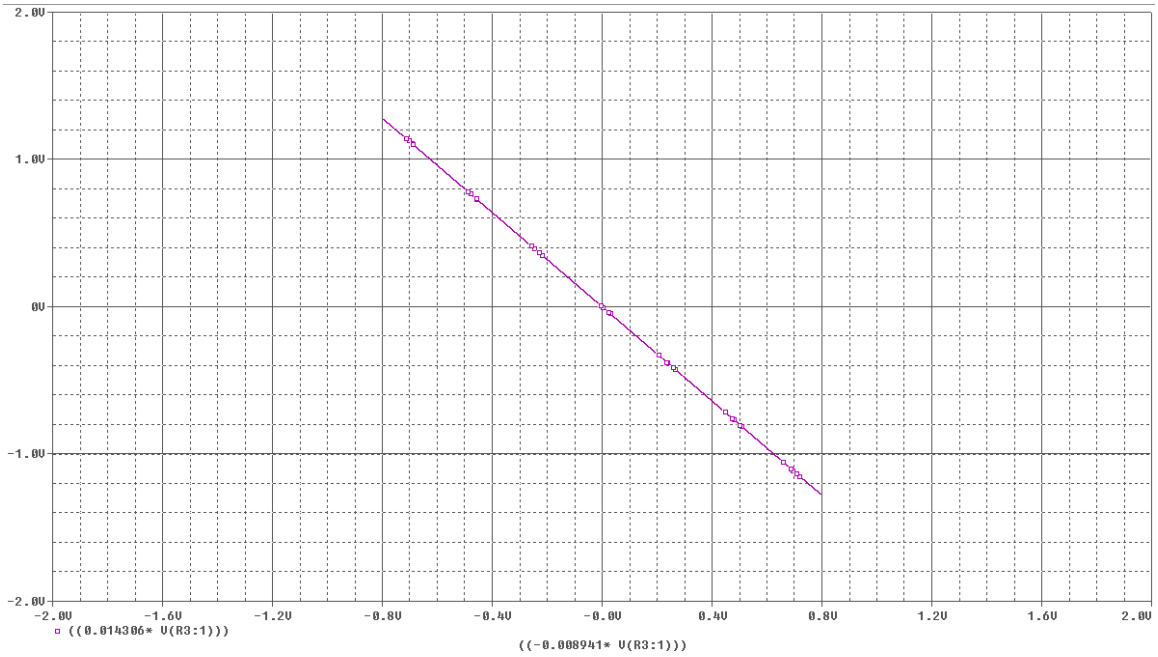

Figure 5.11: PSpice Three Phase Transmission H_c Magnetic Field Intensity

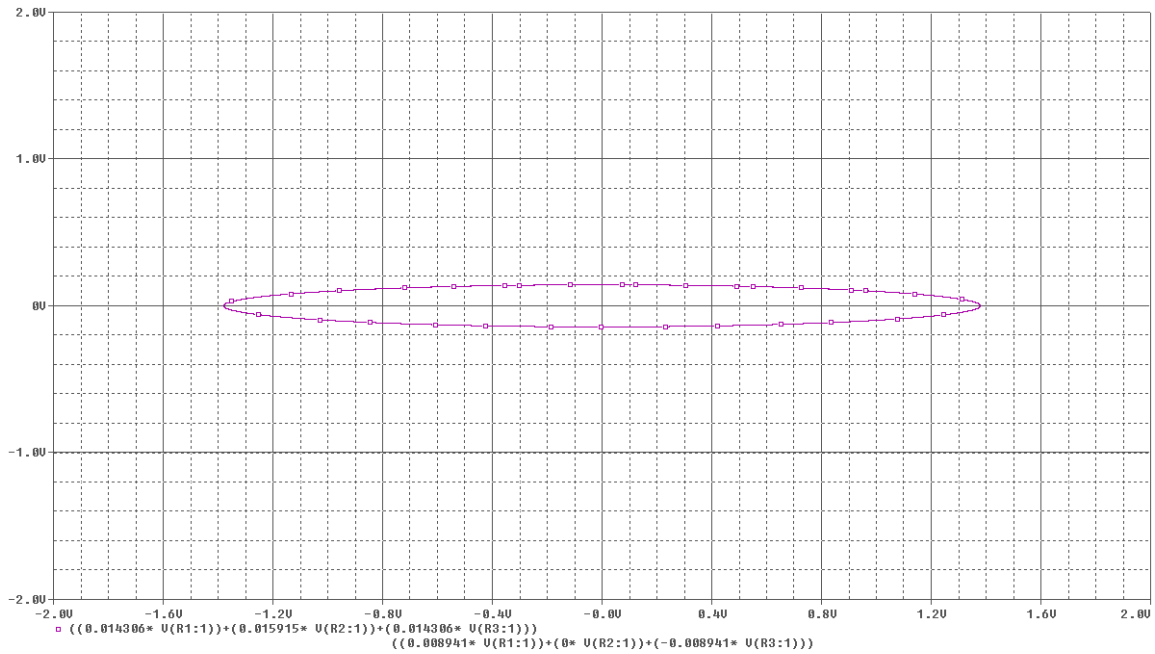

Figure 5.12: PSpice Three Phase Transmission $H_{x,total}$ and $H_{y,total}$ Magnetic Field Intensity

The comparison of the change in the ellipse of Figure 5.12 to the phase to ground, two phases to ground, three phase to ground, and phase to phase follows. (Refer to Appendix D for the PSpice schematics for the simulations.)

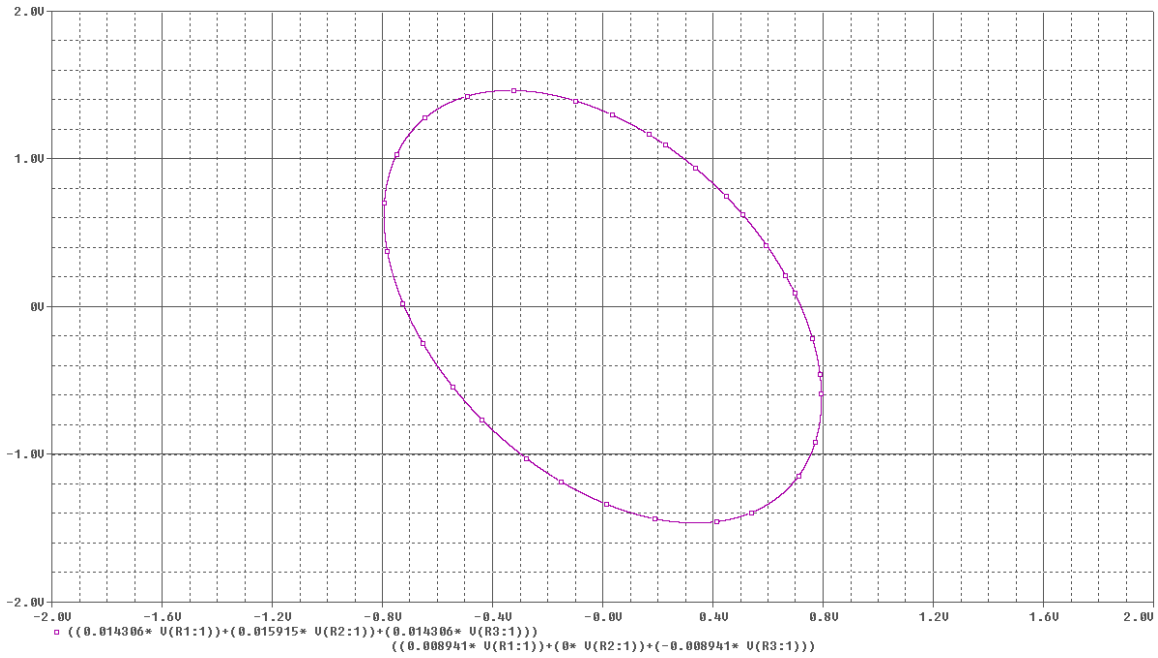

Figure 5.13: PSpice Phase A to Ground $H_{x,total}$ and $H_{y,total}$ Magnetic Field Intensity

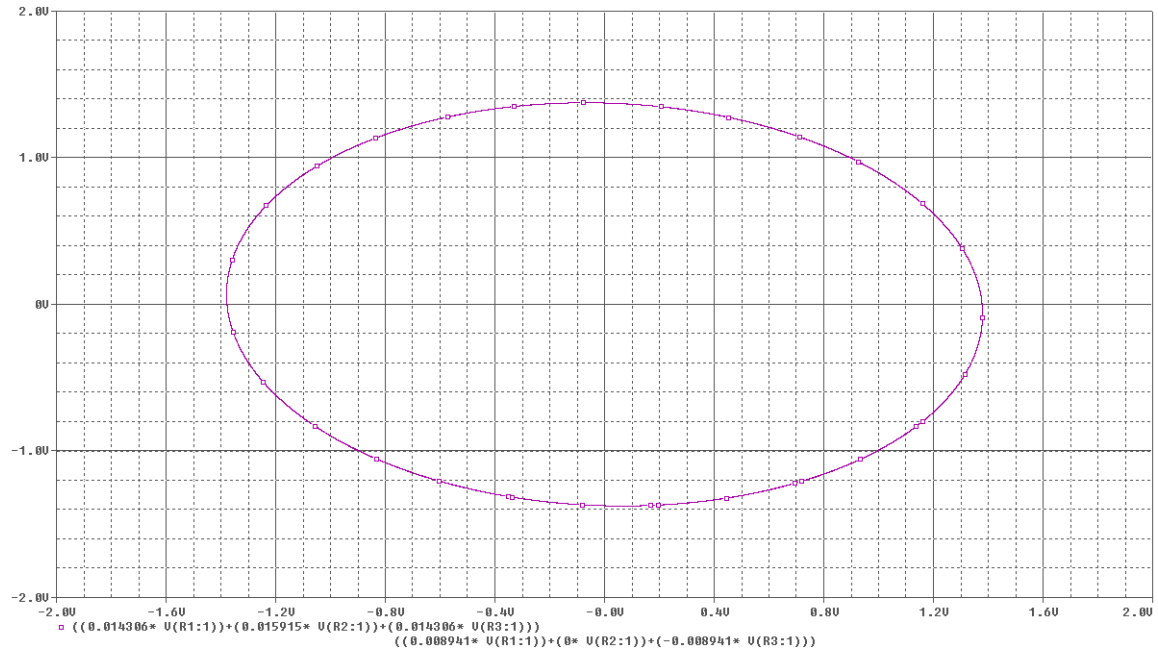

Figure 5.14: PSpice Phase B to Ground $H_{x,total}$ and $H_{y,total}$ Magnetic Field Intensity

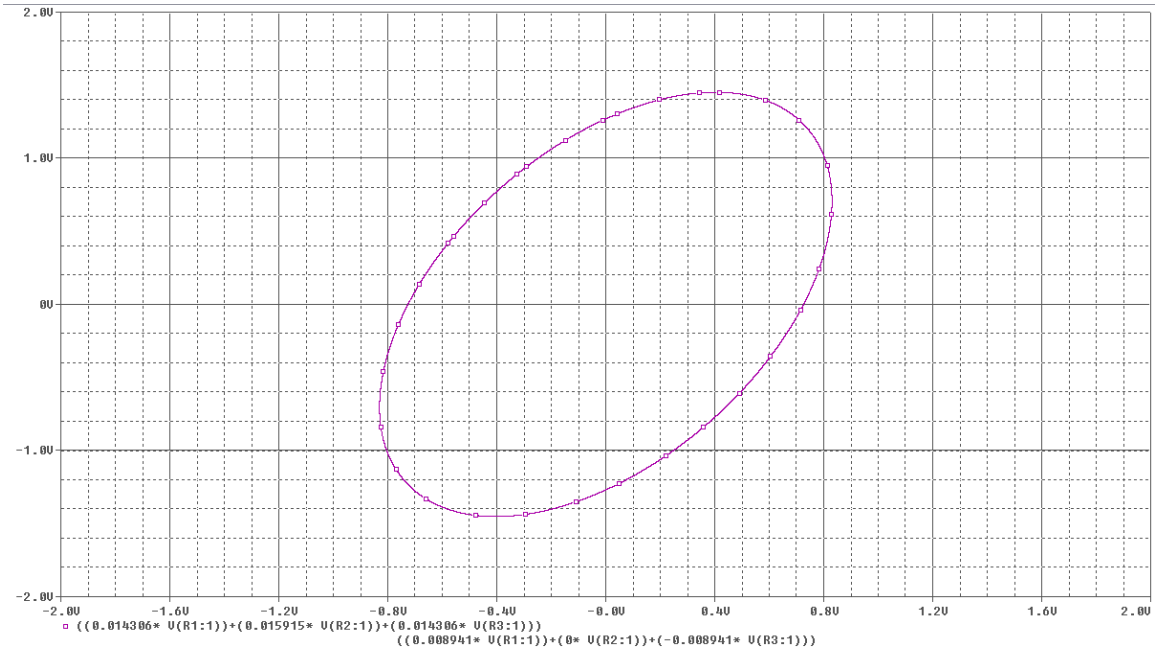

Figure 5.15: PSpice Phase C to Ground $H_{x,total}$ and $H_{y,total}$ Magnetic Field Intensity

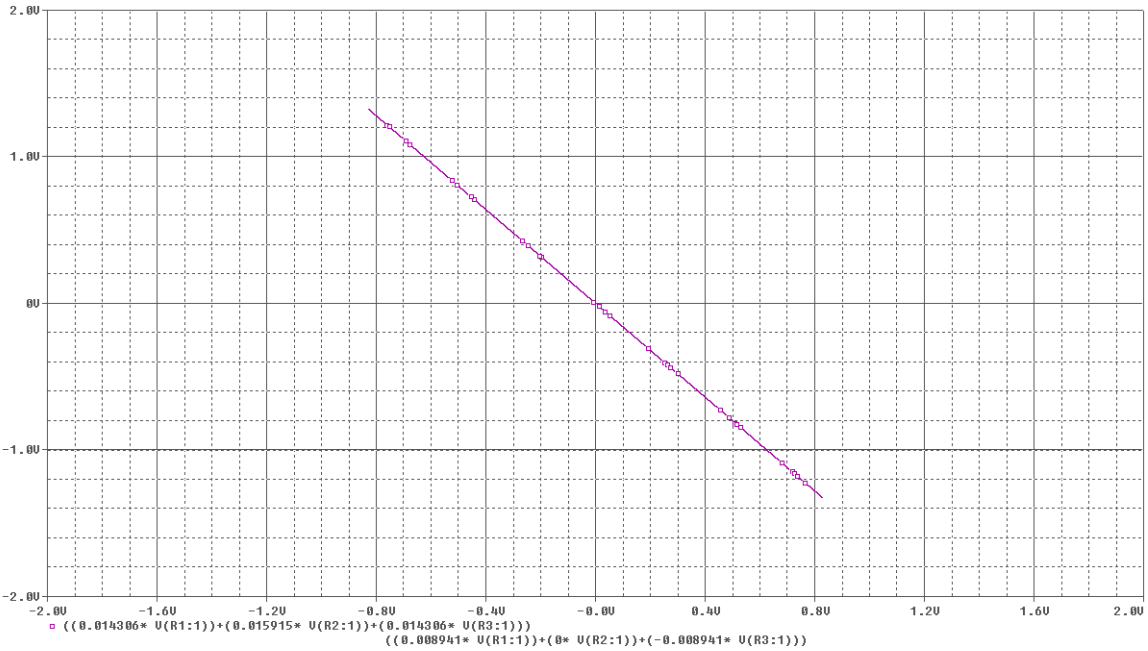

Figure 5.16: PSpice Phase A to Phase B to Ground $H_{x,total}$ and $H_{y,total}$ Magnetic Field Intensity

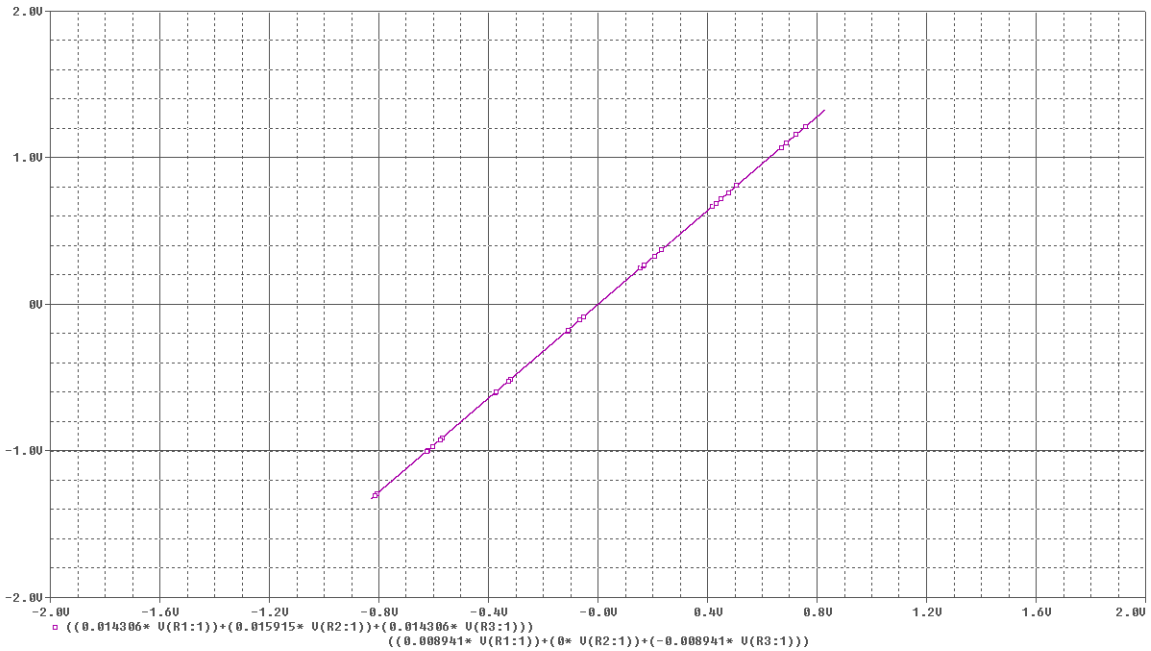

Figure 5.17: PSpice Phase B to Phase C to Ground $H_{x,total}$ and $H_{y,total}$ Magnetic Field Intensity

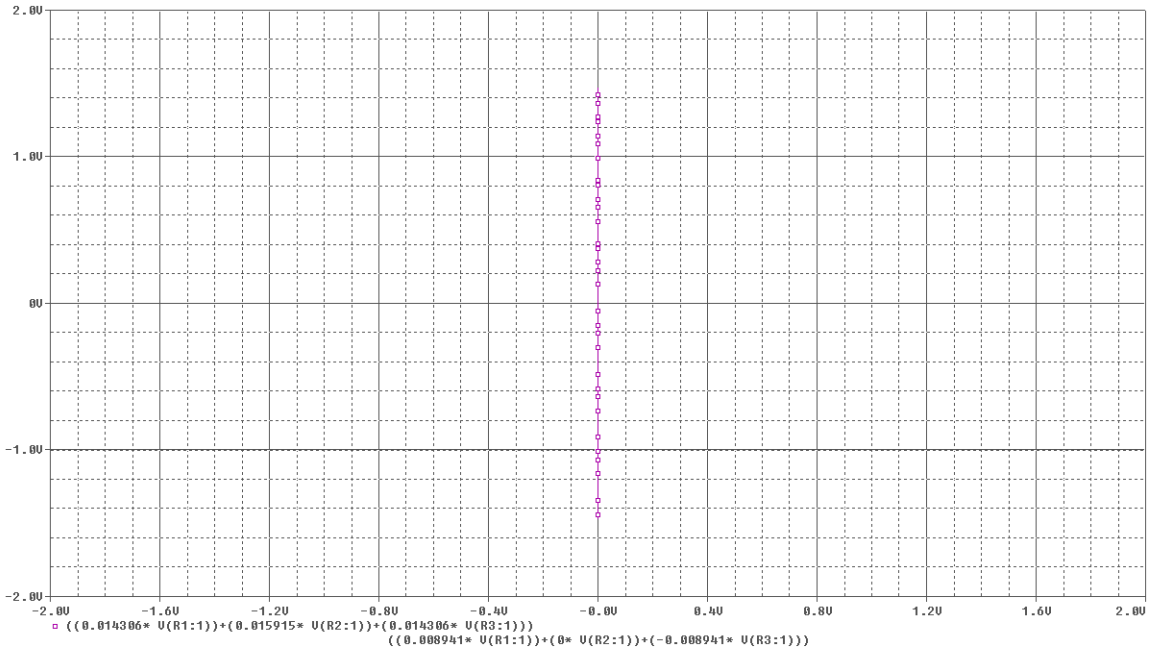

Figure 5.18: PSpice Phase A to Phase C to Ground $H_{x,total}$ and $H_{y,total}$ Magnetic Field Intensity

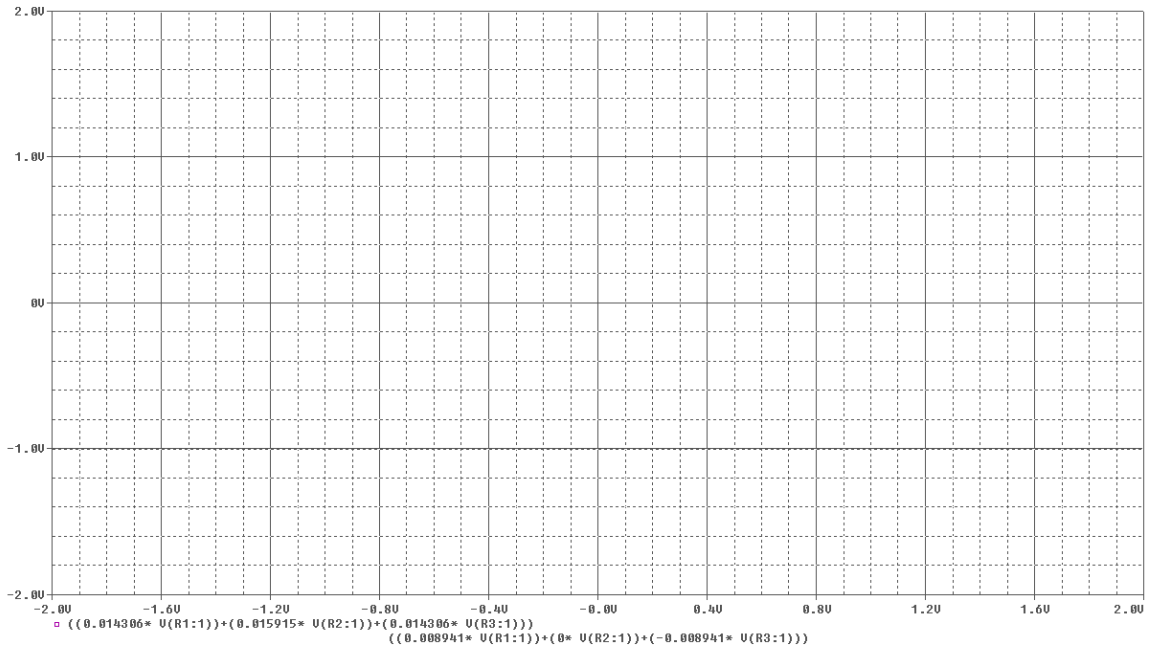

Figure 5.19: PSpice Three Phase to Ground $H_{x,total}$ and $H_{y,total}$ Magnetic Field Intensity

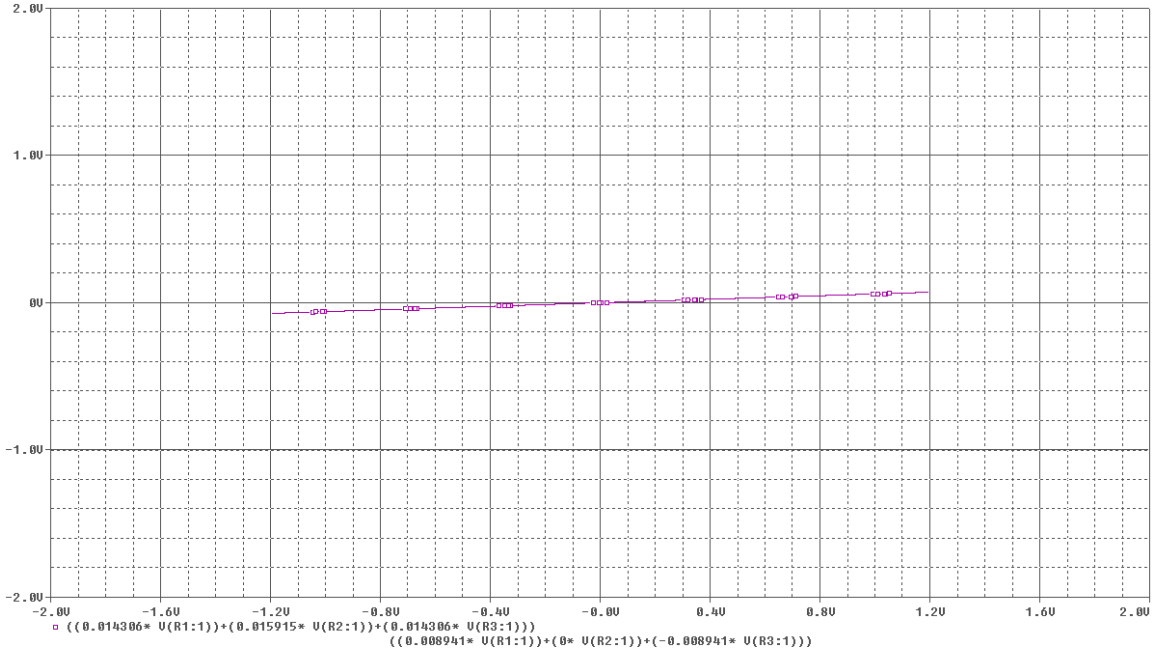

Figure 5.20: PSpice Phase A to Phase B $H_{x,total}$ and $H_{y,total}$ Magnetic Field Intensity

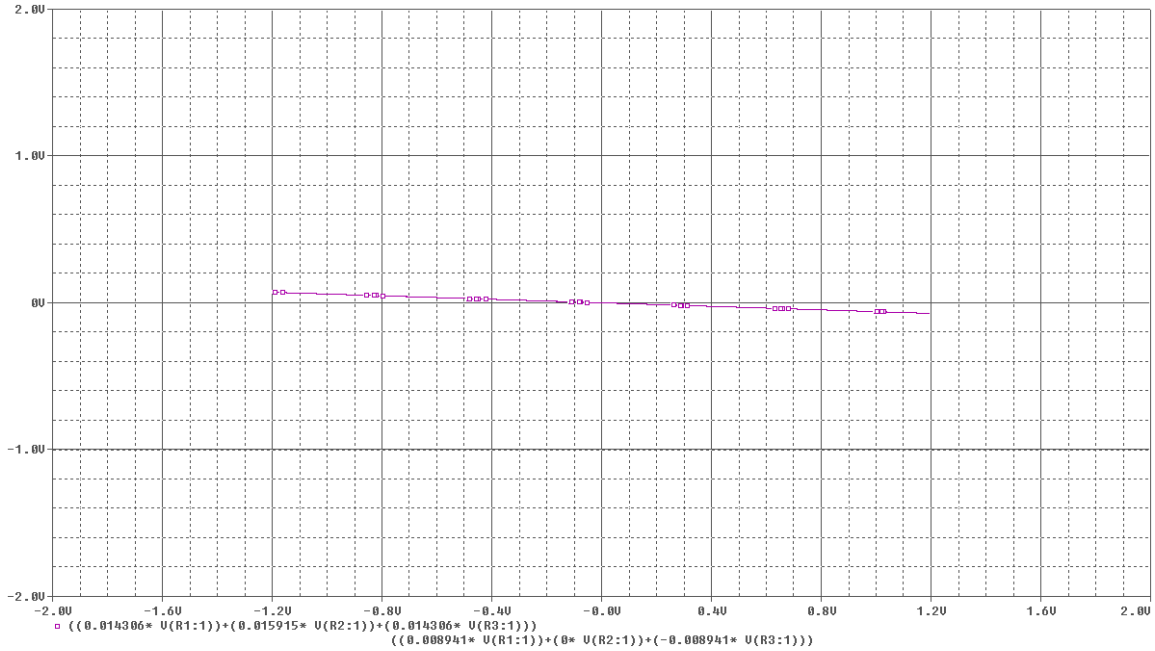

Figure 5.21: PSpice Phase B to Phase C $H_{x,total}$ and $H_{y,total}$ Magnetic Field Intensity

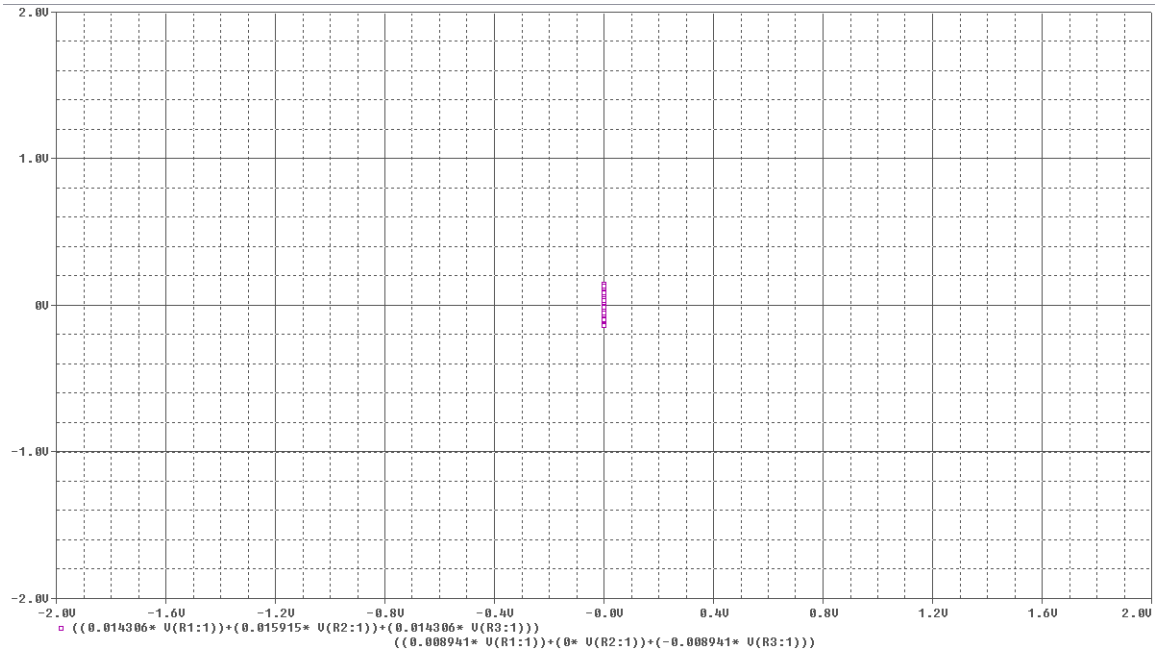

Figure 5.22: PSpice Phase A to Phase C $H_{x,total}$ and $H_{y,total}$ Magnetic Field Intensity

Note that for each of these faults, a unique pattern is displayed by the graph. These patterns can be compared to a measured and plotted value allowing for the determination of the type of fault.

5.2 Fault Locator

The simulation and analysis of the fault locator is modeled after the proposed scheme as depicted in Figure 4.16 and Table 4.4. Since the same method applies to single phase and three phase systems, only a one line system is presented.

For simulation, variables that are assumed to be known for the system's design are assigned values as shown in Figure 5.23 and Table 5.4. These variables include the total length of the transmission line between fault locator stations (L), traveling speed of a signal ≈ speed of light (c), initial detection time (t_0), and second detection time (t_x).

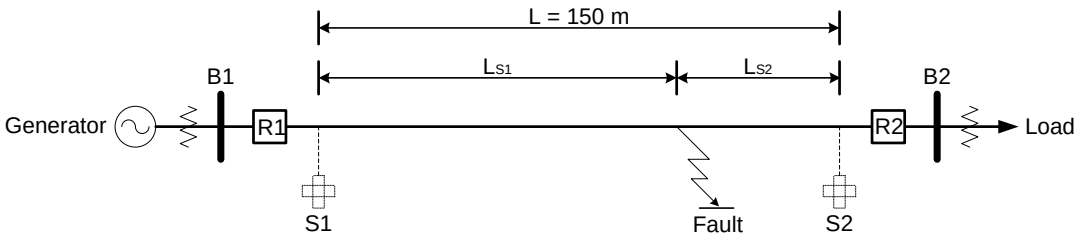

Figure 5.23: Fault Location Scheme in a Transmission System

Table 5.4: Components in Fault Location Scheme

Dimension Symbol	Dimension Value	Dimension Units
L	L = 150	m
c	c = 299.79 x 10^6	m/s
t_0	t_0 = 0	ns
t_x	t_x = 400.35	ns

Using the values for the variables in Table 5.4, the other necessary parameters can be calculated for simulation of the fault locator. The difference in detection time (Δt) between t_0 and t_x is determined by Equation 4.37 as shown in Equation 5.21.

$$\Delta t = t_x - t_0 = 400.35\text{ns} - 0\text{ns} = 400.35 \quad \text{(ns)} \tag{5.21}$$

By substituting the known total length of the line (L) and traveling speed of a signal (c) into Equation 4.39, the total time for a signal to travel the length of the transmission line (t_{total}) is found by Equation 5.22.

$$t_{total} = \frac{L}{c} = \frac{150\text{m}}{299.79 \times 10^6\ \text{m/s}} = 500.35 \quad \text{(ns)} \tag{5.22}$$

Once Δt and t_{total} are calculated, the time between the fault occurrence and its initial detection (Δt_i) as given in Equation 4.40 results in that of Equation 5.23.

$$\Delta t_i = \frac{t_{total} - \Delta t}{2} = \frac{500.35\text{ns} - 400.35\text{ns}}{2} = 50.00 \quad \text{(ns)} \tag{5.23}$$

As discussed in the design of the fault locator, the time of between the fault generation and fault locator stations S1 and S2 in Equation 4.41 and Equation 4.42 respectively, must then be calculated in order to determine the distances between each of the stations and the origin of the fault as given in Equation 4.45 and Equation 4.46. The substitution of previously calculated variables into Equation 4.41 and Equation 4.42 (as respectively shown in Equation 5.24 and Equation 5.25) generates values used in solving Equation 4.45 and Equation 4.46 (as respectively shown in Equation 5.26 and Equation 5.27).

$$t_{S1} = \Delta t + \Delta t_i = 400.35\text{ns} + 50.00\text{ns} = 450.35 \quad \text{(ns)} \tag{5.24}$$

$$t_{S2} = \Delta t_i = 50.00 \quad \text{(ns)} \tag{5.25}$$

$$L_{S1} = \frac{Lt_{S1}}{t_{total}} = \frac{(150\text{m})(450.35\text{ns})}{500.35\text{ns}} = 135.01 \quad \text{(m)} \tag{5.26}$$

$$L_{S2} = \frac{Lt_{S2}}{t_{total}} = \frac{(150\text{m})(50.00)}{500.35\text{ns}} = 14.99 \quad \text{(m)} \tag{5.27}$$

This mathematical simulation of the fault locator is based entirely on calculations of the model of Figure 5.23 and its parameters in Table 5.4. Therefore, the evaluation of its performance is analyzed using an equation that verifies the calculated distances between each of the fault locator stations and the origin of the fault. As shown in Figure 5.23, the lengths L_{S1} and L_{S2} between the fault origin and locator stations are equal to the total length of the line. The summation of the two calculated distances is given in Equation 5.28.

$$L_{check} = L_{S1} + L_{S2} = 135.01\text{m} + 14.99\text{m} = 150.00 \quad \text{(m)} \tag{5.28}$$

The verification of L_{S1} and L_{S2} as defined by L_{check} in Equation 5.28 is equal to the transmission line's total length as given in Table 5.4, both having a value of 150m. This equation confirms the accuracy of the fault locator simulation.

6 Conclusions and Future Recommendations

By applying Faraday's law and Ampere's law, magnetic sensors can be used to detect and identify types of faults. By plotting the magnetic field intensities for each type of fault, a unique pattern is displayed that can be used to differentiate any sensed fault based on the induced voltages. These sensors can also be used to determine the location of the fault along the transmission line. This proposal is based on sensors that are ideal and can read the exact field strength. A survey of available industry sensors is recommended along with appropriate testing to evaluate sensor sensitivity, repeatability, and accuracy. In theory, this approach for detecting, classifying, and locating faults is attainable. The only limitation is hardware capability and performance. When these hardware values are obtained, more accurate simulation can be performed to validate this proposal.

References

[1] Abraham, Spencer, Secretary of Energy. National Transmission Grid Study Issue Papers. U.S. Department of Energy. 2002.

[2] Abraham, Spencer, Secretary of Energy. National Transmission Grid Study. U.S. Department of Energy. 2002.

[3] Bouthiba, Tahar. "Fault Location in EHV Transmission Lines Using Artificial Neural Networks." International Journal of Applied Mathematics and Computer Science 14.1 (2004): 69-78.

[4] Chen, Zhihong, and Jean-Claud Maun. "Artificial Neural Network Approach to Single-Ended Fault Locator for Transmission Lines." IEEE Transactions on Power Systems 15.1 (2000): 370-375.

[5] Das, Biswarup, and J. V. Reddy. "Fuzzy-Logic-Based Fault Classification Scheme for Digital Distance Protection." IEEE Transactions on Power Delivery 20.2 (2005): 609-616.

[6] Galijasevic, Zijad, and Ali Abur. "Fault Area Estimation via Intelligent Processing of Fault-Induced Transients." IEEE Transactions on Power Systems 18.4 (2003): 1241-1247.

[7] Hambley, Allan R. Electical Engineering Principles and Applications. 2nd ed. New Jersey: Prentice-Hall, Inc., 2002.

[8] Lee, C. J., J. R. Shin, and Z. M. Radojevie. "A New Two-Terminal Numerical Algorithm for Fault Location, Distance Protection, and Arcing Fault Recognition." IEEE Transactions on Power Systems 21.3 (2006): 1460-1462.

[9] Lee, Harry. Development of an Accurate Transmission Line Fault Locator Using the Global Positioning System Satellites. B.C. Hydro and Power Authority. Burnaby, B.C. Canada. 197-204.

[10] Salat, Robert, and Stanislaw Osowski. "Accurate Fault Location in the Power Transmission Line Using Support Vector Machine Approach." IEEE Transactions on Power Systems 19.2 (2004): 979-986.

[11] Sauhats, Antans, and Marija Danilova. "Fault Location Algorithms for Super High Voltage Power Transmission Lines."

[12] Traveling Wave Fault Location in Power Transmission Systems. USA: Hewlett Packard Company, 1997.

[13] United States Department of Energy, and Federal Energy Regulatory Commission. United States. Cong. Steps to Establish a Transmission Monitoring System for Transmission Owners and Operators Within the Eastern and Western Interconnections. Section 1839 of the Energy Policy Act of 2005. Washington: GPO, 2006.

[14] Webster, John G. "Fault Location." Wiley Encyclopedia of Electrical and Electronics Engineering. New York: John Wiley & Sons, Inc., 1999.

[15] Zimmerman, Karl, and David Costello. Impedance-Based Fault Location Experience. Schweitzer Engineering Laboratories, Inc. Pullman, WA USA: SEL, 2004. 1-27.

Appendices

Appendix A – List of Symbols

Symbol	**Symbol Description**	**Units**
ϕ	Magnetic Flux	Wb
A	Surface Area	m^2
B, B	Magnetic Flux Density	$Wb/m^2 = T$
N	Number of Turns in a Magnetic Coil	turns
λ	Flux Linkages in Magnetic Coil	Wb · turns
e , v, V	Induced Voltage in Magnetic Coil	V
H, H	Magnetic Field Intensity	A/m
μ	Magnetic Permeability of Material	Wb/Am
I, i	Current	A
r	Radius	m
ϕ	Phase Angle	Degree (°)
l, L	Length	m
h	Height	m
d	Distance	m
α	Length Measurement ℓ Angle of Approach	Degree (°)
t	Time	s
ω	Frequency	rad/s
c	Wave/Signal Propagation	m/s

Appendix B – List of Constants

Symbol	**Symbol Description**	**Value**	**Units**
μ_0	Magnetic Permeability of Free Space	$4\pi \times 10^{-7}$	(Wb/Am)
c	Speed of Light	299.79 x 10^6	(m/s)

Appendix C – Single Phase RMS Voltages Graph Data

Imax	Vrms,x	Vrms,y
0	0.000	0.000
1	0.063	0.063
2	0.125	0.125
3	0.188	0.188
4	0.251	0.251
5	0.314	0.314
6	0.376	0.376
7	0.439	0.439
8	0.502	0.502
9	0.565	0.565
10	0.627	0.627
11	0.690	0.690
12	0.753	0.753
13	0.816	0.816
14	0.878	0.878
15	0.941	0.941
16	1.004	1.004
17	1.066	1.066
18	1.129	1.129
19	1.192	1.192
20	1.255	1.255
21	1.317	1.317
22	1.380	1.380
23	1.443	1.443
24	1.506	1.506
25	1.568	1.568
26	1.631	1.631
27	1.694	1.694
28	1.756	1.756
29	1.819	1.819
30	1.882	1.882
31	1.945	1.945
32	2.007	2.007
33	2.070	2.070
34	2.133	2.133
35	2.196	2.196
36	2.258	2.258
37	2.321	2.321
38	2.384	2.384
39	2.447	2.447
40	2.509	2.509

Appendix D – PSpice Phase to Ground Schematics

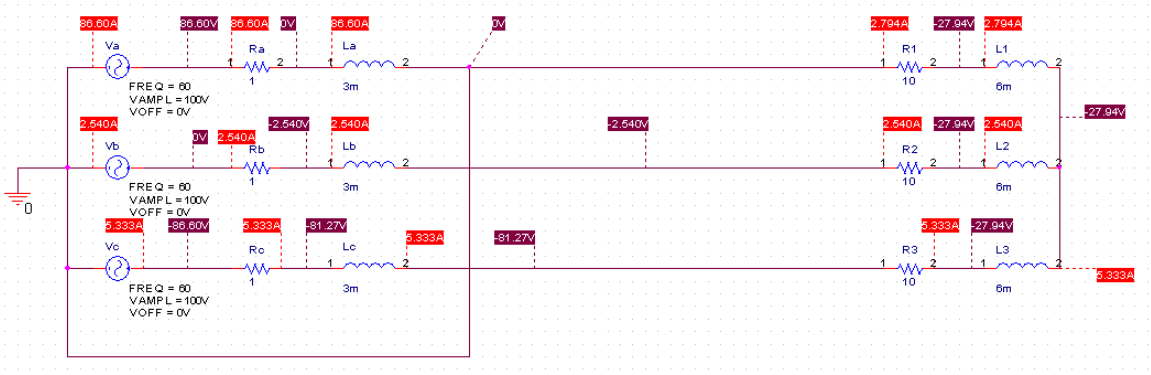

Phase A to Ground Schematic

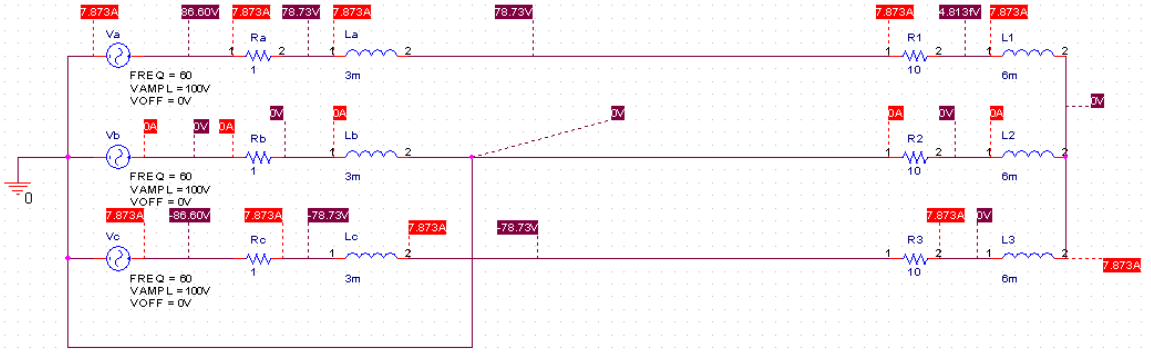

Phase B to Ground Schematic

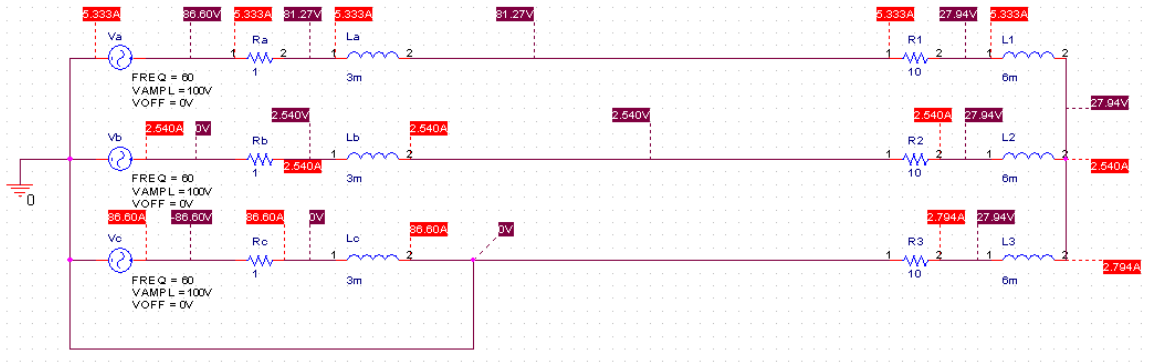

Phase C to Ground Schematic

Appendix E – PSpice Two Phase to Ground Schematics

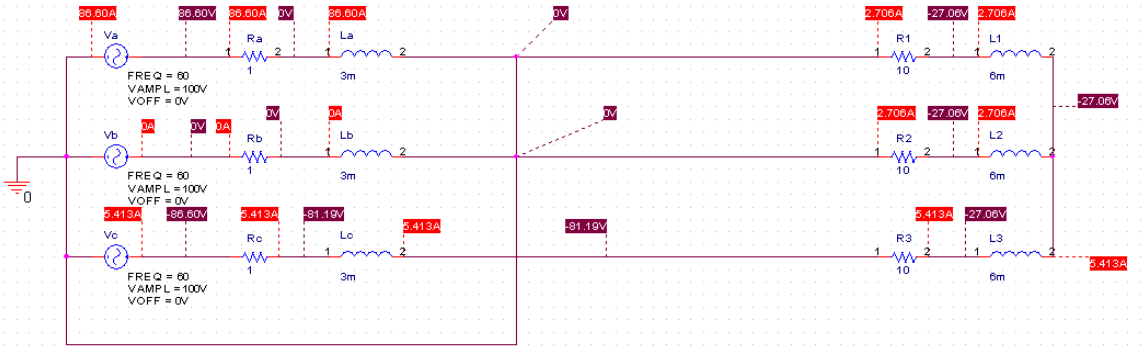

Phase A to Phase B to Ground Schematic

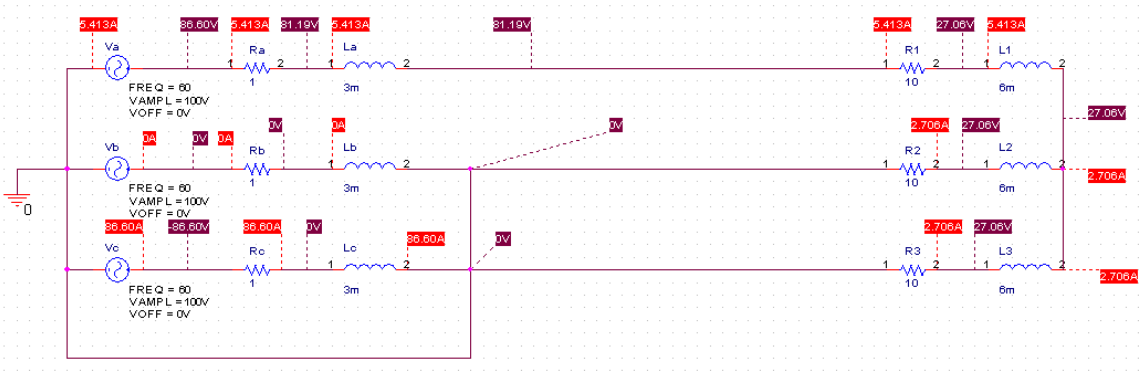

Phase B to Phase C to Ground Schematic

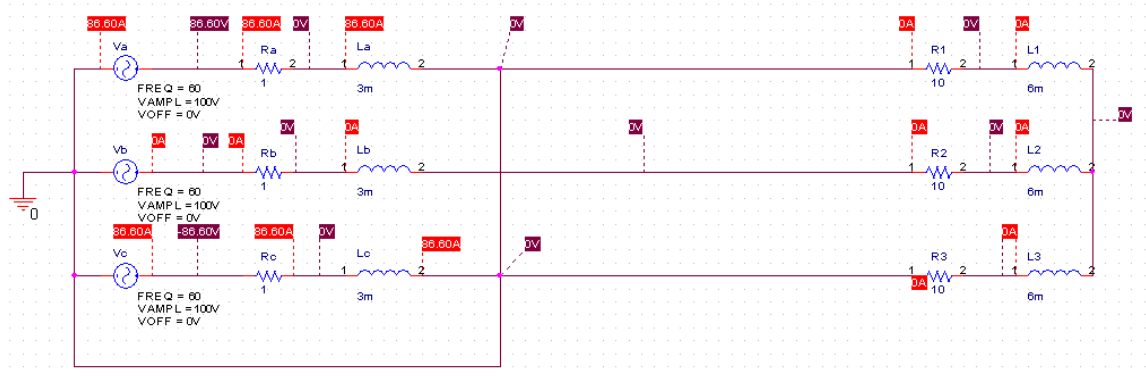

Phase A to Phase C to Ground Schematic

Appendix F – PSpice Three Phase to Ground Schematic

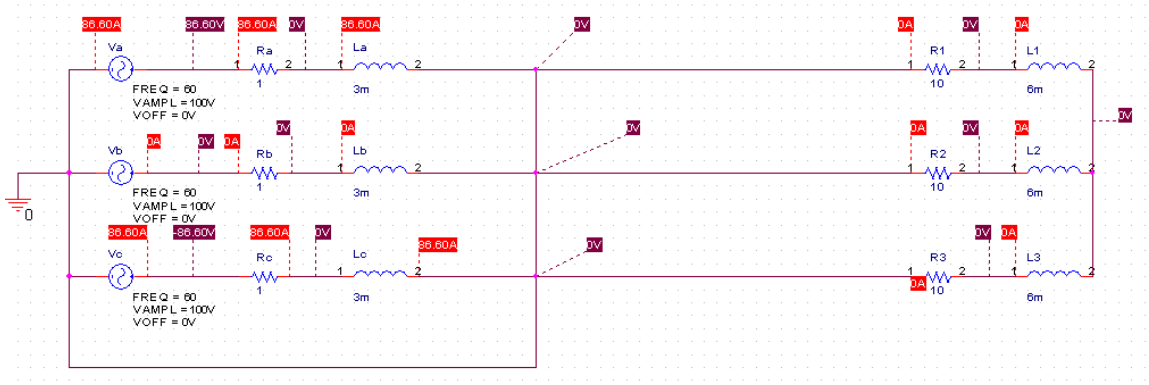

Three Phase to Ground Schematic

Appendix G – PSpice Phase to Phase Schematics

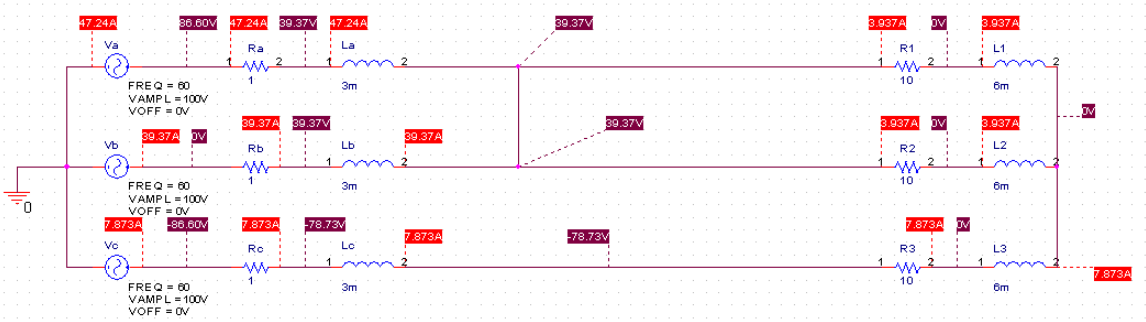

Phase A to Phase B Schematic

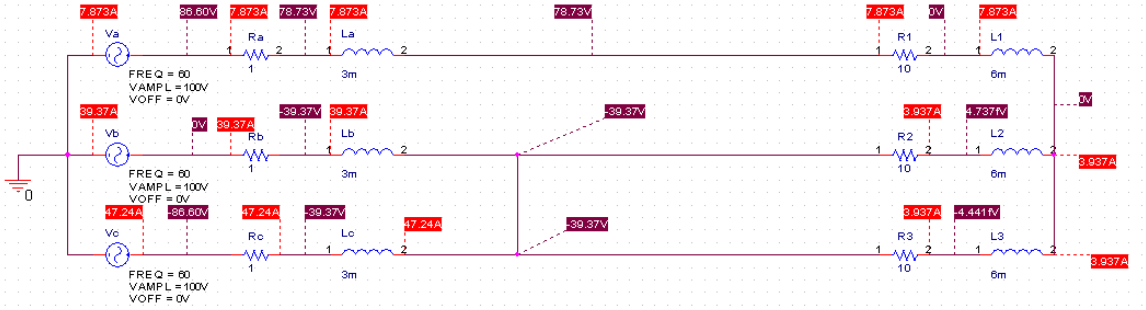

Phase B to Phase C Schematic

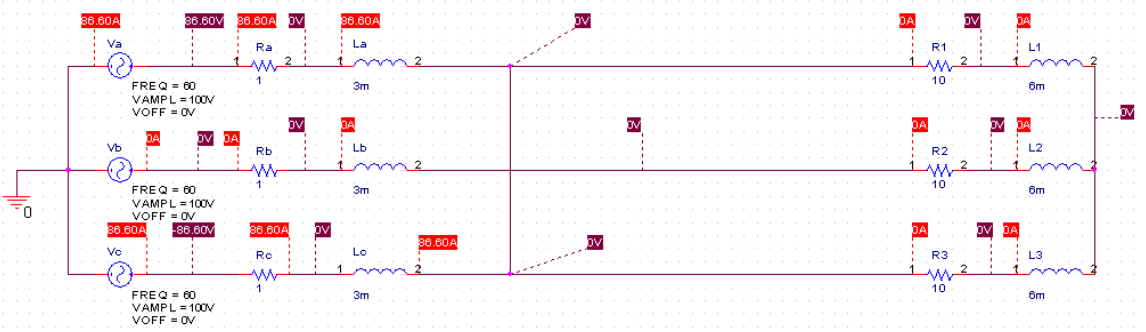

Phase A to Phase C Schematic